Master Thesis

Extraction of energy and time from pile-up pulses with fast sampling ADC analysis techniques

Anton Roth

Nuclear Physics Division

Supervisors: Luis G. Sarmiento and Dirk Rudolph

June 16, 2016

LUNDS UNIVERSITET
Lunds Tekniska Högskola

Abstract

Debates of whether $Z = 114$ and $N = 184$ are the next magic numbers in nuclear physics have existed since the earliest predictions made in the 1960s. Until these days they have not been firmly established. To get a better understanding of the magic numbers, it is of key importance to study the nuclei in the vicinity of established and anticipated shell closures. Above shell closures, fast α-decaying nuclei with half-lives down to tens of nano seconds exist. Due to their short lifetimes, it has been difficult to measure their properties as α-decays result in pile-ups with an analogue electronics experimental set-up.

Fast sampling ADCs have recently been employed in nuclear physics experiments and they have made it possible to extract energies and times of pile-ups with tailor-made algorithms. For the superheavy element 115 experiment, conducted in 2012 by the Lund University Nuclear Structure Group, the employment of fast sampling ADCs was the case. Besides element 115 (E115) decay chains, many short-lived α-decaying transfer reaction products were detected.

In this work, the digital pulse processing and in particluar the moving window deconvolution algorithm, which is used to determine amplitudes from digitised preamplifier signals, are employed to study those short-lived α-decaying nuclei. A unique pile-up trace analysis routine is developed to extract the energies and times from the preamplifier traces and is applied to the experimental data.

From the obtained results a connection to the tabulated α-decay chain of Ra-219 to Rn-215 could be firmly established. The α-decay energy values and coincident γ rays agreed with the tabulated data while the obtained half-life was improved. A decay level scheme could be created on the basis of this work.

With the established decay path, this thesis establishes the proof-of-concept of energy and time extractions with a digital pulse processing system with an algorithm routine to study the properties of very short-lived α-decaying nuclei. There is a lot of data left to be analysed and potentially new decay paths can be discovered or improve assessed branching ratios.

Keywords: Superheavy elements, digital pulse processing, short-lived nuclei, α-decay, moving window deconvolution & decay paths.

Preface

This work was made the first half of 2016 at the Nuclear Physics Division in Lund as part of the Nuclear Structure group. I would like to direct a thanks to the nuclear physics division for welcoming me with open arms. As part of the thesis, in the beginning of June, I was given the honour of participating in the Nobel Symposium on Chemistry and Physics of Heavy and Superheavy Elements which took place in the north-east of Skåne. Furthermore, I also got the possibility to visit the GSI Helmholtzzentrum für Schwerionenforschung in Darmstadt, Germany, and taking part in an experiment on the superheavy element 113. These two trips have given me experiences which I am very grateful for and will always remember.

I am first and foremost grateful to my supervisors Luis G. Sarmiento and Dirk Rudolph for giving me the possibility to take part of the exciting research in the superheavy element science field and for always being there when I had questions. I would like to show my gratitude to Ulrika Forsberg for a very helpful PhD-thesis and valuable talks concerning the pulse shape analysis and Pavel Golubev who assisted with important knowledge concerning experimental set-up details. I am grateful to Christian Lorenz and Natasa Lalovic for great Linux and programming assistance. The workplace was shared with fellow master's students Daniel Söderström and Jacob Snäll whom I would like to thank for valuable discussions and for an enjoyable working environment. Lastly I would like to thank my family and especially my fiancé, Ulrica, for her unconditional support.

Popular Scientific Summary

Development of a novel generic algorithm for pulse shape analysis to study very short-lived nuclei

Anton Roth

To obtain a better understanding of radioactive nuclei, one can study their decay properties, such as decay modes, energy of emitted radiation and half-life. However, some nuclei are much more short-lived than others and have been difficult to study with -now outdated- analogue electronic techniques. Recently, modern digitising electronics, denoted fast sampling ADCs, together with tailor-made algorithms have paved the way for the study of fast decaying nuclei. The development of one of such algorithms and the application of it to experimental data are the main tasks of the thesis.

Atomic nuclei consist of a number of protons, Z, and a number of neutrons, N. Together, they are called nucleons and govern the structure and property of an atomic nucleus. The combination of experimental data and theoretical models is the basis for our understanding of the atomic nucleus. Many nuclei are unstable and decay to a more stable state. From an experimental point of view, it is important to measure the properties of that decay. Decays can occur in different ways, through decay modes, such as, emission of an α-particle, β-decays and decay by emission of a γ ray. The energy and the lifetime of the decay from unstable nuclei are examples of important properties of a nuclear state.

A basic principle of the measurement of energy of α-particles is the use of a semiconductor-based detector. The interaction between the ionizing particle and the semiconductor material creates many free charge carriers that can be collected as a current pulse. The amplitude of the pulse is proportional to the total collected charge in a preamplifier circuit which in turn is proportional to the energy of the ionizing particle. Samples of three preamplifier pulses are illustrated in the upper left inset of Figure 1. The lifetimes of the α-decaying nuclei, can be deduced from the time difference between the start of the different subsequent pulses.

The short lifetimes of certain nuclei have made them difficult to measure. This is because two (or more) α-decays very close in time could result in so called pile-ups with an analogue electronics experimental set-up. That is, the two (or more) decays are treated by the system as a single decay and results in corrupted data.

Fast sampling Analog-to-Digital converters, fADCs, have been recently employed in nuclear physics experiments and they have made possible to extract energies and times of pile-up signals with tailor-made algorithms. One of the main tasks of the thesis was to develop and implement such an algorithm. The other main task was to apply the algorithm to readily available experimental data from an experiment with the purpose of studying superheavy nuclei. The experiment was led by the Nuclear Structure Group from Lund University in November 2012 at

the GSI Helmholtzzentrum für Schwerionenforschung in Darmstadt, Germany. The synthesis of superheavy nuclei is very unlikely and most of the recorded data is, in a sense, undesired. However in the data set there are many of those pile-up pulses from fast subsequent α-decays which have not been analysed before. This thesis deals with the analysis of those potentially interesting *undesired* pulses.

The developed algorithm to treat the pile-ups was based on a method called Moving Window Deconvolution which is illustrated in Figure 1. The method consists of three steps, *i*) First the exponential decay of the signal is compensated for with a deconvolution. *ii*) A differentiation is performed to separate pulses. *iii*) A moving average is applied to the signal in order to remove noise, which results in a trapezoid. The energy of a pulse is extracted as the height of the resulting trapezoid.

The developed pile-up routine was successfully applied to the experimental data. From the analysis a connection to the tabulated α-decay path of ^{219}Ra to ^{215}Rn could be firmly established, see Figure 2. The α-decay energy values agreed with the tabulated ones. A half-life of 2 μs was obtained with the newly developed algorithm and coincides within statistical uncertainties with the tabulated value. The decay path was confirmed by α-γ coincidences.

With the firmly established decay path, this thesis sets the proof-of-concept of energy and time extractions with a digital pulse processing system with a more generic algorithm to study the properties of very short-lived α-decaying nuclei. There is more data left to be analysed and new decay paths are being searched for.

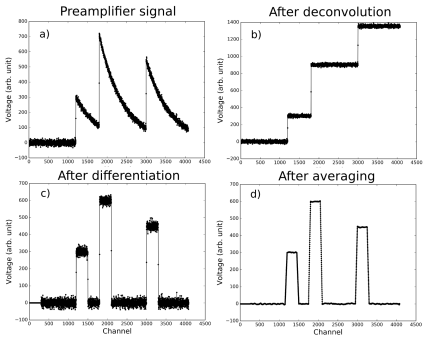

Figure 1: **(a)** A preamplifier pile-up signal with three pulses. **(b)** Deconvolved signal. The result of the deconvolution is three plateaus. The height of the last plateau corresponds to the sum of the amplitudes of all three pulses. **(c)** The differentiation resulting in three square-like pulses. The height of the square-like pulse represents the amplitude of the corresponding original one. **(d)** Averaged signal.

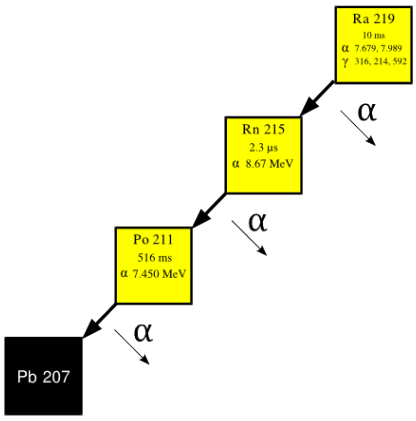

Figure 2: Tabulated α-decay path of Ra-219. The yellow filled squares indicate the α-decaying mode. The black filled square indicates that the nucleus is stable towards any decay. Previously measured data of α-decays, half-lives and γ-rays, relevant to this work, are presented within the respective boxes. If not explicitly indicated, the energy of the emitted α-particle is presented in MeV and the emitted γ ray in keV.

Contents

Abbreviations

SHE	SuperHeavy Element
E115	Element 115 (the element with 115 protons)
ADC	Analogue to Digital Converter
TRP	Transfer Reaction Product
DSSSD	Double Sided Silicon Strip Detector
HPGe	High Purity Germanium
MWD	Moving Window Deconvolution
TASCA	TransActinide Separator and Chemistry Apparatus
TASISpec	*TAS*CA in Small *I*mage mode *Spec*troscopy

Chapter 1

Introduction

In nuclear physics, atomic nuclei having the following $N, Z = 2$, 8, 20, 28, 50, 82 and $N = 126$ display an enhance in stability. These are called magic numbers (indicated in Figure 1.1) and are nucleon compositions that assume a special gain in binding energy and hence become more stable [1]. Some theories exist concerning the evolution of the magic numbers towards the superheavy elements, SHE, such as $Z = 114$ and $N = 184$ [2]. However, these have not been firmly established. Superheavy are those elements with the number of protons, Z, exceeding 103.

In November 2012 an experiment at the GSI Helmholtzzentrum für Schwerionenforschung was conducted in Darmstadt, Germany. The experiment was led by a group of scientists from Lund. The aim of the experiment was to get a first glimpse of the nuclear structure along α-decay chains originating from superheavy elements (SHE) [3,4]. Alpha-decay chains are sequences of α-decays all originating from the same mother nucleus. In the conducted experiment, a beam of ^{48}Ca impinged on a target material of ^{243}Am to create the element with $Z = 115$, E115 (recently suggested the name Moscovium), through a fusion-evaporation reaction. The detector set-up was developed by the nuclear structure group in Lund. It consisted of different semiconductor detectors based on silicon and germanium with the purpose of detecting α-particles and photons, respectively. Alpha-photon coincidence spectroscopy was successfully performed. For the first time, a measure of energy levels provided detailed nuclear structure information in the superheavy element region.

There is a very low production cross section for creating SHE and only 30 decay chains were proposed to originate from E115 in the experiment. The stored data was mostly the result of background radiation. This background radiation stems primarily from other nuclear reaction products which reached the detector set-up. The creation of these reaction products could probably be a result of nucleon transfers between the beam and the target material. In this process typically the target material transferred some of its nucleons to the beam such that isotopes, denoted transfer reaction products (TRPs), more neutron deficient were produced [5].

The basic principle of energy measurements of ionizing particles, such as photons and α-particles, with semiconductor detectors is the following: The interaction between the ionizing particle and the semiconductor material induces a current pulse which is collected. After the current pulse has been processed by a preamplifier its pulse amplitude is proportional to the total collected charge which in turn is proportional to the energy of the ionizing particle.

Fast sampling ADCs directly connected to the preamplifiers were employed for the core

silicon detectors in the E115-experiment. The preamplified signals were digitised directly and recorded in traces which contained 4000 samples which corresponded to a time of ~ 70 μs. The experiment proceeded for over two weeks with an event rate of ~ 100/s and a large volume of data was generated.

Most of the reaction products from the E115-experiment are TRPs which are heavy actinides (elements with $89 \leq Z \leq 103$) and unstable and therefore decay to lighter nuclei. As they do so, they approach the $Z = 82$, $N = 126$ magic numbers north-east to the doubly magic $^{208}_{82}\mathrm{Pb}_{126}$ nucleus in the chart of nuclides. Due to this, α-decays have short half-lives (down to a few ns). These fast decaying nuclei are indicated in Figure 1.1. The subsequent fast α-decays result in pile-ups with analogue pulse processing electronics. Pile-up signals appearing when two or more events occurring in the detector within a very short range of time, on the order of μs, cannot be treated in a good way with former analogue electronics. As a consequence, times and energies are not measured correctly and information is typically lost. However, with modern fast sampling ADCs, as the ones employed in the E115-experiment it is possible to store digitised traces and perform offline processing of all detector signals. Software algorithms enable a more detailed analysis of pile-up signals and, consequently a proper discrimination of α-decay energies and half-lives of short-lived nuclei.

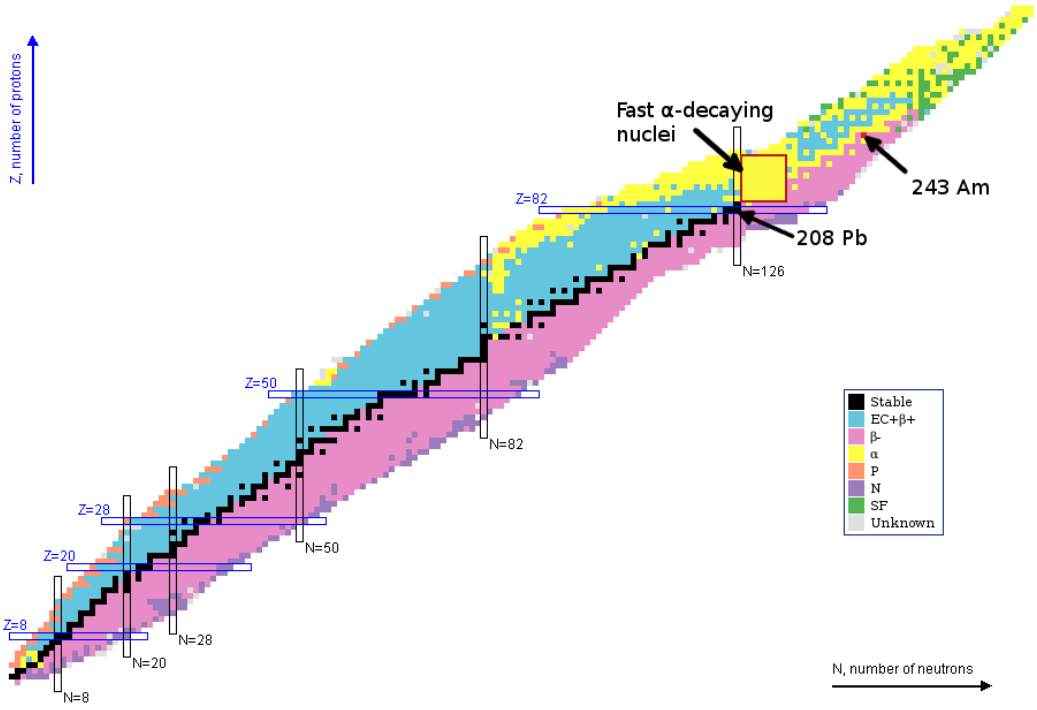

Figure 1.1: The chart of nuclides. Each small square represents a known atomic nucleus. The different colours indicate the preferred decay mode of a given nucleus. The legend shows all the decay modes. Here EC+β^+ stands for electron capture and β^+ decays. P and N are decays by emission of a proton or a neutron, respectively. SF is short for spontaneous fission. The nuclides with proton and/or neutron magic numbers can be found within blue and black marked regions. The target material ^{243}Am is marked in the figure with a red square. The region with the fast α-decaying nuclei north east of the double magic $^{208}_{82}\mathrm{Pb}_{126}$ nucleus is indicated with a large red box. The image has been modified from Ref. [6].

In order to improve the understanding of the nuclear structure of superheavy nuclei,

another experiment was recently conducted at GSI. In this experiment the short-lived new uranium isotope ^{221}U was created through a fusion evaporation reaction of ^{50}Ti on ^{176}Yb and studied with a detector set-up connected to a fast electronics system similar to the one used for the E115-experiment. Since known and expected half-lives of these isotopes and their daughters were very short it was necessary to employ fast sampling ADCs to extract the α-decay energies and half lives of the uranium isotopes. This was achieved with dedicated software algorithms and obtained half-lives for ^{221}U and ^{222}U were 4.7(7) μs and 0.66(14) μs, respectively [7]. This work sets the scene of energy and time extraction of pile-up pulses with a fast sampling ADC analysis.

In this thesis that technique is further investigated, improved and employed to the large data set of the E115-experiment. The measurements on some of the short-lived α-decaying isotopes above the $Z = 82$ and $N = 126$ magic numbers were established before the 1990s, such as e.g. in Ref. [8,9]. With the modern fast sampling ADCs and improved detectors the former measured data should be able to be improved. Potentially, better α-decay energies, more reliable half-lives or not yet discovered decay modes can improve the understanding of the underlying nuclear structure of these unstable nuclei.

Due to the transmission of many different reaction products in the E115 experiment, the data complexity is large. Said complexity constitutes a serious analysis challenge and demands a state of the art data analysis approach.

Objectives

The objectives of the master thesis are:

- Develop a general method in which amplitudes and times of the pulses in pile-up traces can be determined. This aim is split into these tasks:
  - Characterise the many different types of traces in the E115-experiment. These are single-pulse traces, pile-up traces and others.
  - Implement a filtering method which identifies pile-up traces.
  - Develop a general method in which amplitudes and times of the pulse/pulses in the traces can be extracted.
- Examine the performance with energy resolutions and statistics of the newly developed pile-up method applied on the E115-experiment data.
- Set the path to determine the characteristics of the fast α-decaying nuclei in the E115-experiment obtained with the developed pile-up routine.
  - Derive the α-particle energies.
  - Determine the half-lives of the fast α-decaying nuclei.
  - Compare the obtained results with established data to possibly find hitherto unknown decay paths.

Outline

Initially the basic principles of semiconductor detectors, which are one of the corner stones in the E115-experiment, are described thoroughly. This is followed by a detailed description of the different electronic components which are connected to the semiconductor detectors and how these are employed in order to measure energy, both with analogue electronics and modern digitising techniques. In Chapter 3 the fundamentals of the E115-experiment are presented. Here everything from the basic idea of the experiment, reaction products, set-up, data acquisition to the data-analysis process is briefly described. The core concept of digital pulse processing, the moving window deconvolution algorithm, which is the main ingredient in the pile-up analysis routine, is described in detail in Chapter 4. A description of the implementation of the pile-up routine follows in Chapter 5. The results of the developed pile-up routine applied to E115-experimental data is given in Chapter 6. The report is rounded off with a comprehensive discussion.

Chapter 2

Experimental techniques

In SHE-experiments, as well as in many nuclear physics experiments, semiconductor detectors are key ingredients. The basics of semiconductors with bandgaps, doping and the pn-junction initiates this chapter. A description of how semiconductors are used in the detection of ionizing radiation follows. Two specialized semiconductor detector types are the Double Sided Silicon Strip Detector (DSSSD) and the High Purity Germanium (HPGe) detectors. These are very important in the SHE-experiments in the detection of α-particles and photons, respectively. This subject concludes the semiconductor detector section.

The last part of the chapter deals with the complete set-up which is employed in the process of extracting energies from semiconductor detectors. The charge sensitive preamplifier plays an important role in this process as it is the first component after the semiconductor detector which the signal reaches. The preamplifier signals can be digitised directly with a digital pulse processing system or instead be treated with further electronic components in an analogue pulse processing system before the digitising step. The two methods and their advantages and shortcomings are described. The chapter is concluded with a description of pile-up pulses which is one of the main topics in this work.

2.1 Semiconductor detectors

Semiconductor detectors are typically based on the elements silicon ($Z = 14$) and germanium ($Z = 32$). These two have in common half-filled outer electron shells, i.e. four valence electrons. They are crystalline materials. In the crystals the atoms form covalent bonds with their four closest neighbours. Due to the periodic structure, semiconductors exhibit an energy band structure wherein the electrons can occupy very closely spaced energy states in the valence band and conduction band. The two bands are separated by an energy gap, denoted bandgap, where no energy states are allowed (see Figure 2.1). A specific property of the semiconductors is the small bandgap in difference to conductors, which have no gap, and the insulators, which have a very large gap. This feature enables a control over the conducting properties of the semiconductors.

Doped semiconductors, i.e. crystals into which impurity atoms have been introduced, are especially important in semiconductor detectors. The impurity atoms have one more or one less valence electron than the semiconductors. These are called donor and acceptor impurities, respectively. Examples of donors are arsenic, phosphorous and antimony. Acceptor elements are, for instance, gallium, boron and indium. In the case of donor impurities, the

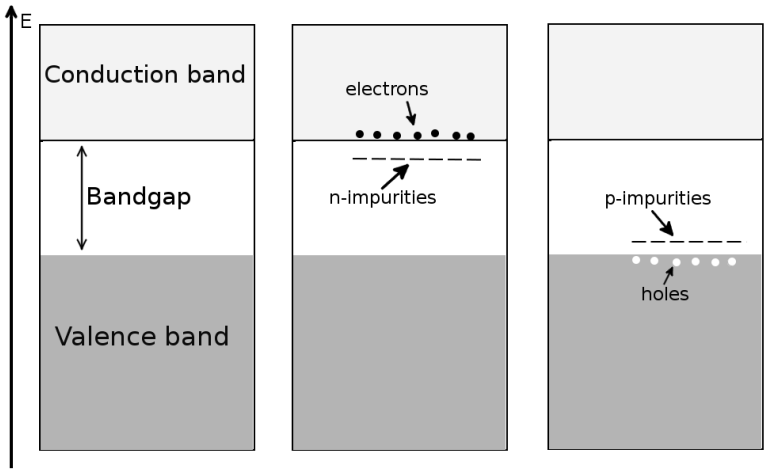

Figure 2.1: Energy band structure of semiconductors. The white area, in the bandgap, indicates energies without states. The darker grey region indicates very densely occupied energy states in the valence band and the lighter grey region in the conduction band illustrates free states. The middle and right panels illustrate the impurity levels of an n-doped and p-doped semiconductor, respectively.

extra valence electron is loosely bound in the crystal and occupies an energy state within the bandgap close to the conduction band. On the other hand, acceptor impurities have a hole in the crystal due to the missing electron. There is no strong covalent bond and an energy state in the bandgap close to the valence band is induced [10].

When sufficient donor or acceptor impurities are added to a semiconductor it is said to be n-doped or p-doped, respectively. By bringing together one p-doped and one n-doped semiconductor, a pn-junction is created. This situation is illustrated in Figure 2.2. The pn-junction is the key element in a semiconductor detector. As the p- and n-doped materials are brought together the excess electrons on the n-side diffuse over to the p-side to fill the hole states. While this occurs, an electric field is induced which begins to halt the diffusion process. When an equilibrium has been reached, a potential difference between the sides has been induced. The region in between the two sides, called the depletion region, now consists of immobile charges bond to the covalent bonds, while the n and p-side now holds free charge carriers of electrons and holes, respectively. The width of the depletion region can be increased with an applied reverse bias voltage over the junction. With the reverse bias voltage the electric potential on the p-side is lowered and the electrons and holes are attracted to the p-side and n-side, respectively. The bias voltage prevents a current running through the pn-junction.

The basic principle of the semiconductor detector is that when ionizing radiation interacts with the crystal material, covalent bonds are broken and electrons are excited to the conduction band, i.e. electron-hole pairs are created. If the electron-hole pairs are created within the depletion region these will drift towards different sides of the junction. On the other hand, if the free charge carriers are created outside the depletion region, within the so called dead layer, the electron and hole will recombine. In order to be able to collect the

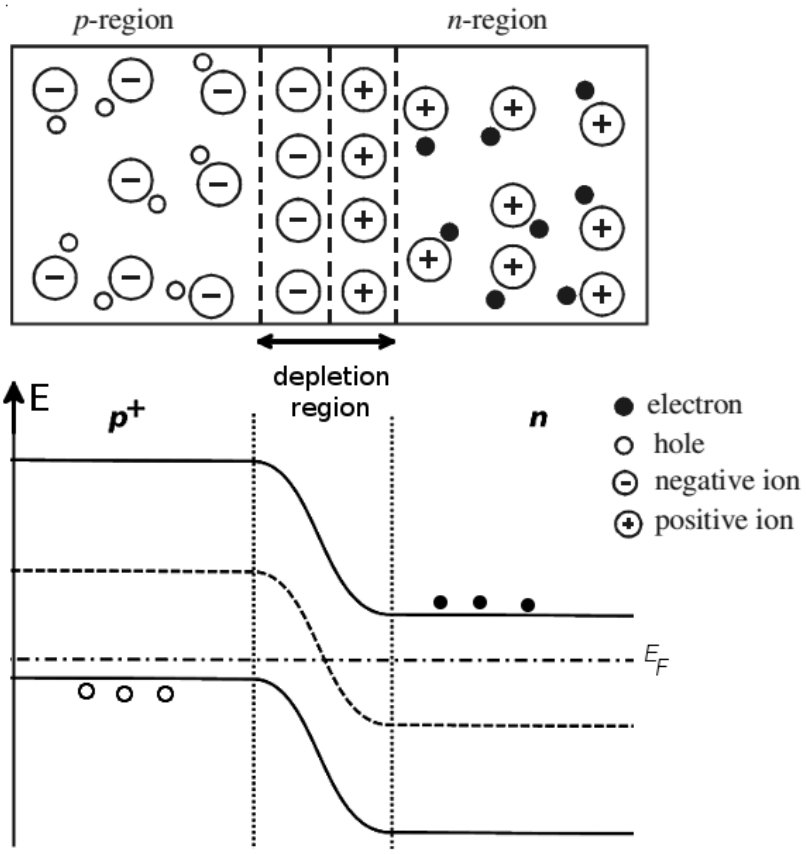

Figure 2.2: Formation of a pn-junction. The top part of the figure illustrates the equilibrium state after a p-doped and an n-doped material have been brought together. Observed is the hole states on the p-side and the electrons on the n-side. The depletion region, indicated with vertical lines, only consists of charged ions. The resulting energy diagram of the pn-junction is presented in the bottom part of the figure. The Fermi energy, E_F, is indicated with a dashed-dotted line. The middle of the bandgap is represented with a dashed line. Modified from [11, 12].

charges at the electrodes before they recombine, a bias voltage is applied over the junction. The created electron-hole pairs by the ionizing particle can now effectively be collected on electrodes. The energy of the ionizing radiation governs how many electron-hole pairs that are created. Thus, the collected charge is proportional to the deposited energy [10, 13].

The current signal, induced by the ionizing particle in the semiconductor detector, can be interpreted as a pulse. The pulse shape is governed by several factors. First of all, it is important to separate the collection of the holes from the electrons as these have different mobilities in the semiconductor material. The location at which the free charge is created with respect to the electrodes governs the drift time, which also affects the current signal. The energy and the type of ionizing radiation also have an impact on the pulse shape. Heavier particles interact mainly through electronic collisions. Electronic collisions are collisions with electrons in the material, which is the dominating interaction. However, for the heavy particles nuclear collisions also occur, and these also increase their stopping power. Furthermore, heavy particles create many electron-hole pairs, dense charge clouds, which increases the probability for recombination. Due to screening in the dense charge

clouds, charge carriers feel a decreased electrical potential and the charge collection time is increased. Together these three phenomena reduce the current signal, hence the detected energies, for heavy particles and can be referred to as the plasma effect. For less energetic decays, such as α-decays, some energy goes into phonon excitations of the semiconductor lattice [13].

2.1.1 Double Sided Silicon Strip Detectors

Double Sided Silicon Strip Detectors (DSSSDs) are position sensitive semiconductor detectors. These are thin detectors, often not thicker than 1 mm. They are electrically segmented into narrow strips. An example of a 4x4 DSSSD is presented in Figure 2.3. n-doped strips (n-strips) are implanted orthogonally to the p-doped strips (p-strips). Each strip is connected to a separate electrode which causes the current by ionizing particles which deposit their energy in the direct vicinity of a strip to only be collected by the corresponding electrode. The entire DSSSD is but one pn-junction.

By cross-checking the signals in the p-strips with those in the n-strips, positional information in 2D of the ionizing radiation can be obtained. Hence, the DSSSD can be said to be divided into pixels [13, 14].

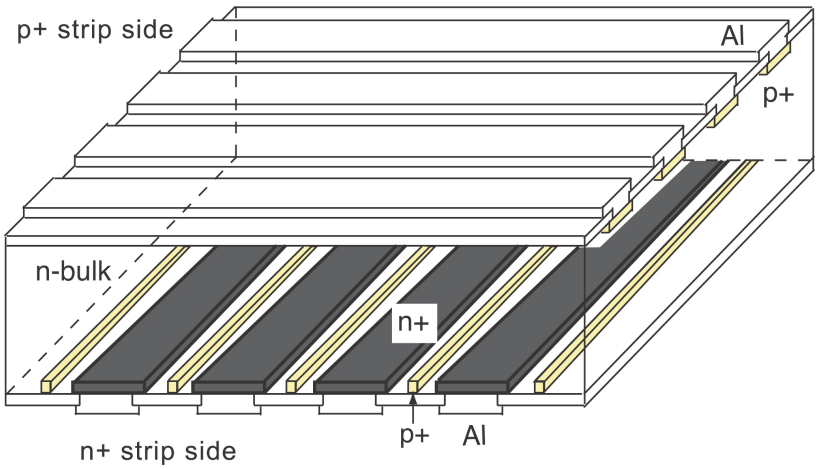

Figure 2.3: Cross-sectional view of a DSSSD. The n-strips (indicated with dark color) are located at the bottom of the image. At the top of the structure the p-strips (in yellow) are orthogonal to the n-strips. Very thin p-strips are placed in between the n-strips to isolate them from each other and improve the electric field in the bulk. Here each strip is coupled to aluminium electrodes. The image is taken from Ref. [14]

2.1.2 HPGe-detectors

High Purity Germanium (HPGe) semiconductor detectors are preferred in the detection of x and γ rays. This is due to the higher Z of germanium compared to silicon which increases the γ-ray interaction probability and thus the electron-hole pair generation. However, because the bandgap in Ge is very small the HPGe detectors have to be cooled down to minimise the leakage current. The leakage current is the current running through the detector when only the HV bias has been applied and perturbs the radiation detection. The small gap has the advantage that electrons are easier excited across the bandgap, which makes the energy resolution very good. This is because there always exists a fluctuation, σ, on the number

of electron-hole pairs, J, that are created. It follows a Poisson distribution, i.e. $\sigma^2 = J$. Hence it is advantageous to have an as large current signal as possible [10].

Modern HPGe-detectors today are often composite, i.e. several Ge crystals composed together in a compact way. This way the solid angle coverage and thus the detection efficiency is improved. Due to the sensitivity of the crystal surfaces they are furthermore also encapsulated within a vacuum aluminium capsule. The two most common composites are the CLUSTER and the CLOVER detectors. The CLUSTER detector is the biggest one with seven closely packed Ge crystals while the CLOVER detector consists of four Ge crystals [15, 16].

2.2 Energy measurements using semiconductor detectors

A typical set-up for detection of ionizing particles with a semiconductor detector is illustrated in Figure 2.4. A high-voltage (HV) bias is applied over the detector, indicated by a diode, to increase the depletion zone to cover the entire volume. As ionizing radiation impinges on the detector, a number of electron-hole-pairs proportional to the deposited energy is generated. Due to the external HV, the charged particles will start to drift and induce a current pulse. A pulse generated from a semiconductor detector typically lasts between 1 ns to 1 μs depending on the type and size of the detector [17].

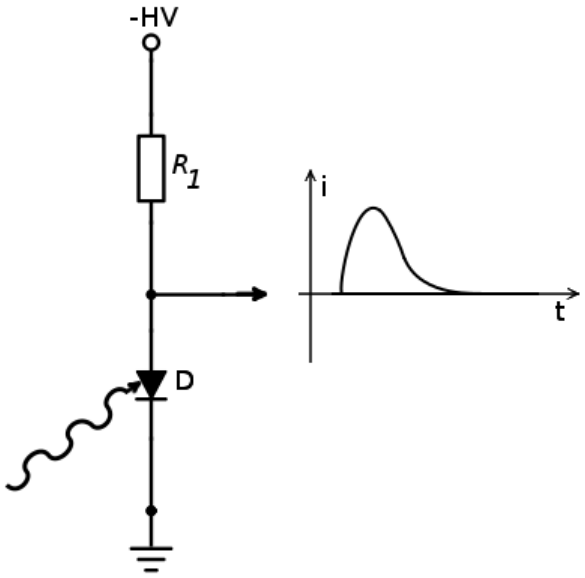

Figure 2.4: Set-up for detection of ionizing particles with a semiconductor detector. The diode D represents the junction in the semiconductor. When an ionizing particle deposits its energy in the detector, electron-hole pairs are created. Due to the HV, the electron-hole pairs drift and a current pulse is induced. A sketched current signal is shown at the right side of the figure. The area under this curve is proportional to the total charge induced by the ionizing particle [17].

The total induced charge by the impinging ionizing particle is the area under the current-pulse curve. To integrate the signal, a charge sensitive preamplifier is employed. Conven-

tionally, the integrated signal is processed by a pulse shaper before the total charge, i.e. the energy deposited by the ionizing particle, is extracted with an analogue to digital converter (ADC) and stored in a multichannel analyser (MCA). With the development of the fast sampling ADCs (also known as direct conversion ADCs and flash ADCs) [18], it is possible to digitise the complete preamplifier output signal. The energy deposited is then extracted with a software algorithm, online or offline. An algorithm based on a method denoted Moving Window Deconvolution (MWD) is typically used.

2.2.1 Charge sensitive preamplifier

The preamplifier is the first electronic component which is connected to the detector. The main purpose of the preamplifier is to integrate the current signal, but at the same time it also amplifies the signal. The preamplifier functions as an extracter of the detected signal to further electronic components. To keep the detector signal as clean as possible, namely to avoid or to suppress noise, the preamplifier circuit is mounted as close as possible to the detector. There exist current sensitive, voltage sensitive and charge sensitive preamplifiers which are employed for different purposes. However, for spectroscopy experiments in which semiconductor detectors are used, the charge sensitive preamplifier is used. The typical circuit of the preamplifier, illustrated in Figure 2.5, is often denoted as an integrator circuit. The induced charge Q_D in the detector charges up the feedback capacitor C_f resulting in an output voltage proportional to the induced charge [17].

Consider Figure 2.5. A capacitor is placed before the preamplifier to block the DC HV component and only transmit the current-pulse as a result of the radiation interaction in the detector [17]. For an ideal operational amplifier, the potential difference between the gates is zero and thus no current will enter the negative gate [19]. Instead the detector current will charge the feedback capacitor to the voltage:

$$V_{\mathrm{C}_f} = \frac{Q_D}{C_f} \tag{2.1}$$

As the current-pulse enters the preamplifier circuit, due to the short duration of the pulse, the feedback capacitor is charged very fast.

Once the capacitor has been charged up, it is discharged by the operational amplifier which works to obtain the same potential on its two gates. The resulting current from the capacitor is:

$$i_{\mathrm{C}_f} = \frac{dQ}{dt} = \frac{\left(dV_{\mathrm{C}_f} C_f\right)}{dt} = C_f \frac{dV_{\mathrm{C}_f}}{dt} \tag{2.2}$$

Since the feedback resistor and capacitor are in parallel, the same voltage V_{C_f} lies over the capacitor and resistor. Therefore the current running through the resistor from the output gate of the operational amplifier is $\frac{V_{\mathrm{C}_f}}{R_f}$. Kirchoff's current law states that the sum of all the currents that leave or enter a node should be equal to zero [19]. Considering node A in Figure 2.5:

$$C_f \frac{dV_{\mathrm{C}_f}}{dt} + \frac{V_{\mathrm{C}_f}}{R_f} = 0 \quad \Leftrightarrow \quad V_{\mathrm{C}_f}(t) = V_{\mathrm{C}_f}(0) e^{-\frac{t}{\tau}} \tag{2.3}$$

The output voltage will at any moment of time be $V_{\mathrm{out}}(t) = -V_{\mathrm{C}_f}(t)$.

In Equation (2.3), $\tau = R_f C_f$ is the exponential decay constant and assuming an instantaneous charge of the capacitor, $V_{\mathrm{C}_f}(0) = \frac{Q_D}{C_f}$. Hence, the preamplifier transforms the

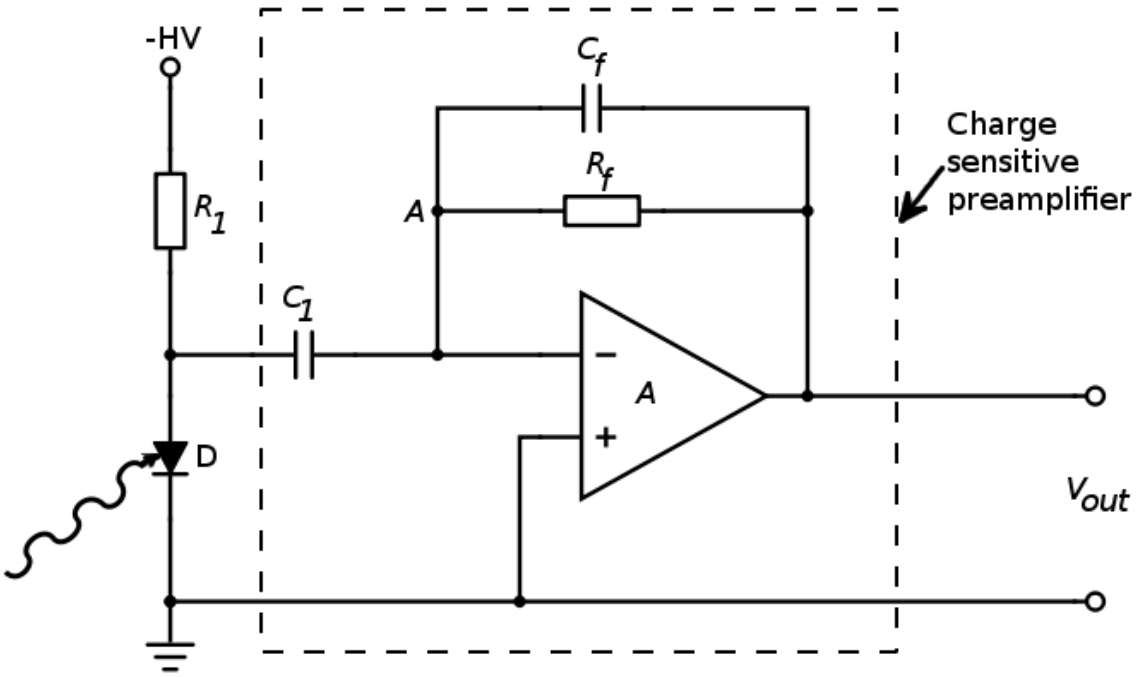

Figure 2.5: The charge sensitive preamplifier (within the dashed rectangle) connected to a semiconductor detector. A high voltage (HV) bias is applied over the semiconductor detector. Resistor R_1 typically has a resistance of 100 MΩ and minimises the current through the detector. Capacitor C_1 is a HV DC blocking capacitor. Due to the high resistance on the negative gate of the operational amplifier the feedback capacitor C_f is charged up. Through the feedback resistor R_f the capacitor is discharged. The amplification factor of the operational amplifier A is usually large, $\sim$ 20 000 [17].

current-pulse to an exponentially decaying voltage signal with a maximum value proportional to the induced charge in the detector by the absorbed radiation.

With a fast sampling ADC the preamplifier signals are recorded in so called traces. An example of a trace is presented in Figure 2.6.

Consider Figure 2.6. The quantity on the x-axis is time and the quantity on the y-axis is values of the digitised voltage. This voltage represents the voltage over the capacitor in the preamplifier circuit which in turn is proportional to the induced charge in the semiconductor detector by an ionizing particle. This preamplifier signal was digitised with a fast sampling 12-bit ADC. To enable pulses with both positive and negative polarities the baseline was positioned in the middle of the range of possible digital values $\sim$ 2000. The sampling frequency used to record this trace was 60 MHz (this corresponds to a time difference of about 17 ns between two subsequent channels) and the number of samples recorded for the trace is 4000. The sample number in a trace is referred to as *channel*.

The rise time in this report is referred to as the time difference between the start of the rising edge and the start of the falling edge. Moreover, it is common that the pulse amplitude is magnified too much only for a few channels and this phenomena is referred to as an overshoot. The overshoot is visible in the trace as those 2-3 samples before the cyan square. In the analysis of the trace it is important to take this into account [10, 20].

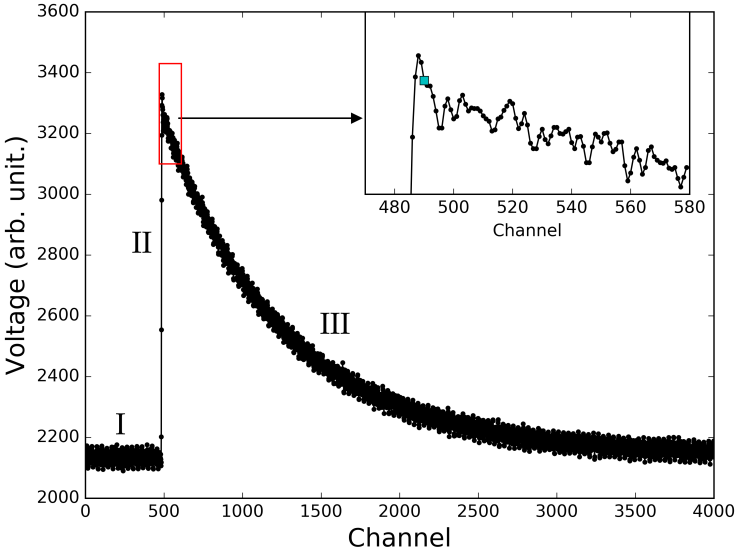

Figure 2.6: A preamplifier trace. Different parts of a trace are referred to as baseline, rising edge and falling edge. The baseline, I, is referred to the value the trace assumes when there is no pulse present, here between channels 0 and 500. The rising edge, II, of a pulse refers to the samples present on the part of the trace where the pulse starts. This part of the pulse could be characterised by the rise time. With the help of the inset at the top right corner it is seen that the rising edge here consists of circa 5 samples. The falling edge, III, is the part of the pulse which assumes the exponential decay, i.e. starting from the channel indicated with a cyan square.

2.2.2 Analogue pulse processing

The flow chart below illustrates the basic principle of a typical analogue pulse processing set-up. It can be split up into two main steps, pulse shaping and analogue to digital conversion.

The signal reaches a pulse shaper after the charge sensitive preamplifier. This pulse shaping is crucial. The exponential decay of the preamplifier signal is theoretically infinite and by construction the decay time constant τ is quite long, typically 50 μs. Therefore, it is likely that before the preamplifier has destabilised, another pulse reaches the preamplifier. This has the consequence that a subsequent pulse is riding on the tail of the preceding pulse and the total height of the second pulse does not correspond to its amplitude. This means, that the maximum voltage of the second pulse will not be proportional to the collected charge due to the ionizing particle. To overcome this problem, the preamplifier pulse is usually shaped to a gaussian-like peak. The duration of the pulses are shortened, the long decay tail of the pulses is removed and thus consecutive pulses are separated. This is done in such a way that the proportionality between the amplitude of the pulses and the induced charge in the detector is preserved. Furthermore, with the pulse-shaping procedure the signal-to-noise ratio is also improved. The pulse shaping is performed with analogue electronic set-ups, such as combinations of CR-differentiators and RC-integrators. For more information on this topic the reader is referred to Ref. [10, 20].

In the next step the amplitudes of the shaped pulses are extracted with an Analogue-to-Digital Converter, ADC. The amplitude is converted to a digital number. There exist different ADC types, for instance, peak sensing and charge sensitive. In the case of charge

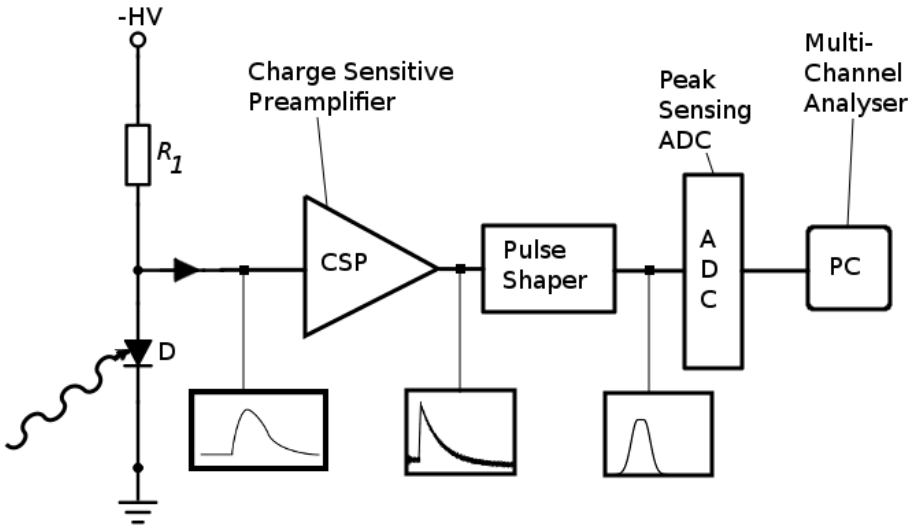

Figure 2.7: Analogue pulse processing set-up. The drawn lines from the squares present the shape of the signal at each stage. The current signal from the semiconductor is first processed by the preamplifier and the resulting signal amplitude is proportional to the deposited energy by the ionizing particle. To shorten the duration of the pulse and improve the signal to noise ratio the pulse is shaped with electronics. The amplitude of the signal is extracted with a peak sensing ADC and stored in a multi channel analyser on a PC. Inspiration to the image is taken from Ref. [21].

sensitive preamplifiers the peak sensing type is employed while the charge sensitive is used in connection to current generating devices, such as photomultiplier tubes.

The peak sensing ADC can be based on different methods. The most common type is denoted successive approximation. The basics of this successive approximation method is the following. An allowed voltage range is determined for the ADC, e.g. 0-10 V. An incoming voltage, say of 8 V, is then compared to reference voltages. If the voltage is higher than the reference voltage the bit of the digitial number is set to 1 and else to zero. First, the voltage is compared to 5 V and the first bit is set to one. Next the voltage is compared to 7.5 V, then to 8.75, then to 8 and then the procedure continues till all 12 bits have been set [10].

The digital number obtained is then typically sent to a MultiChannel Analyser, MCA. The MCA can be considered as a memory base for all the generated numbers from the ADC. It sorts numbers in different channels depending on their amplitude and keeps track of how many enters each channel. Presenting the information contained in the MCA results in the energy spectrum.

The preamplifier signals can vary in amplitude. To be able to extract accurate pulse heights, the signal voltage should be digitised with as many bits as possible. For weak signals ($\sim \mu$V), a high gain, i.e. a significant amplification, is applied to the signal. In turn, for the strong signals, a low gain is applied in order to keep the signal strength inside the ADC allowed voltage range [10].

2.2.3 Digital pulse processing

In the early 1990s the fast sampling ADCs were developed. It became possible to digitise the preamplifier signal directly as illustrated in Figure 2.8. The amplitude and time of the pulses could now be extracted with software algorithms. Depending on the purpose, the pulse analysis could be performed online (as the experiment progressed) or offline with stored traces (i.e. after the experiment).

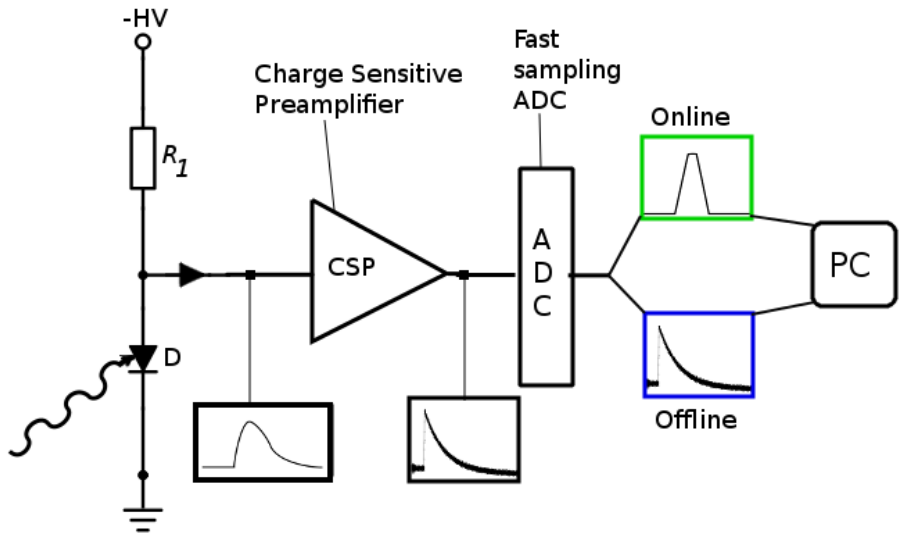

Figure 2.8: Digital pulse processing set-up. The complete signal from the preamplifier is digitised with a fast sampling ADC. The signal can be processed with algorithms directly wherein the amplitude of the pulses are stored, denoted online, or the entire signal is stored in a PC for later processing, denoted offline.

With this development came significant advantages. There are limits when it comes to shaping with analogue circuits that do not exist to a similar extension through digital operations. Every pulse can be saved and treated individually. With the algorithms in the digital pulse processing comes a valuable flexibility. Furthermore, in the analogue case described in the section above, the pulse is processed through several electronic components which is going to perturb the signal. However, with the fast sampling ADCs the pulses only need to be processed by the preamplifier.

It is not appropriate just to calculate the difference between the minimum and the maximum of the preamplifier signal and extract this value as the amplitude of the pulse. This is due to the noise in the signal which suggests some kind of averaging which is able to cancel out the noise by proper optimised software. The most established method to extract the amplitude of digitised preamplifier pulses is the Moving Window Deconvolution algorithm, is described in Section 4 [20].

2.2.4 Pile-ups

In experiments with a detector set-up, which uses analogue pulse processing, pile-ups can occur. Pile-ups are created when two or more particles impinge the detector within a short period of time, i.e. in experiments with a high count rate or with short-lived isotopes.

With the analogue pulse shaping it is possible to extract the energy of pulses with a time-separation of several tens of μs. However, if the time difference approaches ~ 5 μs (also depending on the detector set-up), problems occur [10, 20]. One of the problems is that the shaped pulses will overlap as illustrated in Figure 2.9.

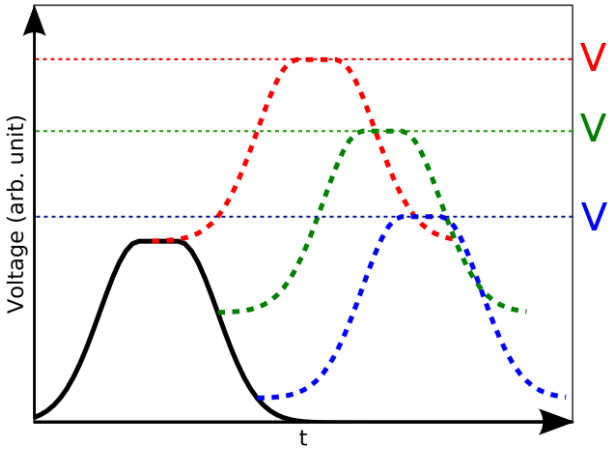

Figure 2.9: Analogue pulse processing and pile-ups. The filled line represents the resulting pulse after analogue pulse shaping of a single-pulse trace. The dashed lines represent pulses occurring subsequently after the first pulse with different time differences. The time difference is the smallest for the red, larger for the green and the largest for the blue line. Due to the small time differences the pulses are not separated in the analogue pulse shaping process and the double pulse is treated as a single pulse. The obtained amplitude in the red case (indicated with a red V) is the sum of the two pulses and for the green and blue the amplitude is less than the sum but larger than the individual amplitude of one pulse [20].

In the case of two overlapping pulses, the system treats the two pulses as one pulse and the obtained amplitude of this pulse will thus be corrupted data. These data are referred to as a pile-ups. Techniques for pile-up rejections with an analogue pulse processing system have been developed. In these methods the different pulse shapes are utilised in order to discriminate the pile-up pulses from the rest. Comparing the rise time or the integrated charge of different pulses are two techniques in use [20]. A typical pile-up preamplifier signal is illustrated in Figure 2.10 [10, 20].

With an analogue pulse processing set-up one loses information about pulses that occur too close in time. The most important possibility that arose with the fast sampling ADCs and digital pulse processing, is the possibility to treat these pile-up traces where the time difference between the pulses is less than 5 μs. Thus, this enables a study of the properties of very short-lived nuclei. Now, the practical lower time-difference limit of amplitude extractions of pile-up traces is governed by the sampling frequency and the charge of the capacitor in the preamplifier circuit. The use of algorithms to obtain the amplitude from the digitally processed pulses and to use it to study short-lived nuclei is the corner stone of this work.

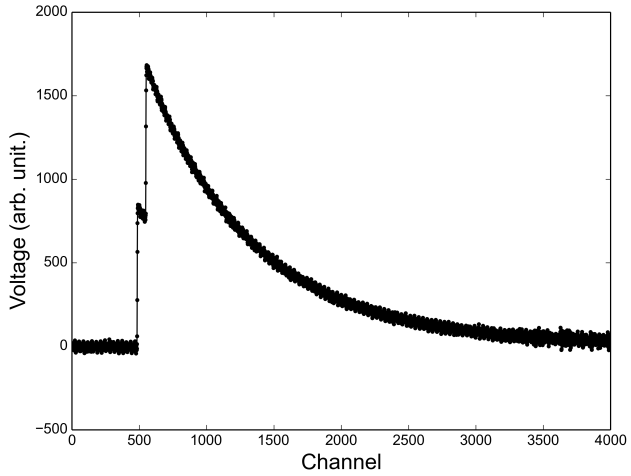

Figure 2.10: A pile-up trace. Two pulses appear so close in time such that the analogue pulse shaping treats them as one pulse with a therefore corrupt amplitude.

Chapter 3

The E115-experiment: set-up and data analysis

The experiment was conducted at the GSI Helmholtzzentrum für Schwerionenforschung in Darmstadt, Germany. The following chapter serves as a short introduction to the whole experiment. Element 115 is created through a synthesis of a beam ion with a target atom in a fusion-evaporation reaction. As a by-product a lot of background radiation is generated. Interesting among these reaction products for this work are transfer reaction products. These two subjects are dealt with at first.

To be able to detect the decays of SHE, the gas filled recoil separator TASCA is employed. With three magnets TASCA is to separate out background reaction products and direct created E115 towards the detector set-up TASISpec. In the end of the chapter the focus lies on TASISpec which was developed in Lund and the idea behind this set-up is presented. The data acquisition system, i.e. how the data, energies and times, are read out is described together with how the offline data analysis is performed. Readers interested in more experimental details are referred to the PhD-thesis by Ulrika Forsberg, Ref. [3].

3.1 Production of element 115

One key aspect of the experiment was obviously to create element 115. This was achieved through a fusion-evaporation reaction where accelerated $^{48}Ca^{8+}$-ions collided with a target foil comprising $^{243}_{95}Am_{148}$. A fusion-evaporation reaction of two nuclei is an interaction that results in a fusion followed by an evaporation of neutrons. The compound nucleus in the fusion reaction is $^{291}115$ and is in an excited state. The theoretical cross section for the $3n$-channel, i.e. the deexcitation through evaporation of three neutrons, is the largest and thus the creation of $^{288}115$ is considered most probable [22].

For the two nuclei, ^{48}Ca and ^{243}Am, to interact with each other, the Coulomb barrier needs to be overcome. This was achieved with a sufficiently high kinetic energy of the ^{48}Ca ion beam. The beam was provided by the Universal Linear Accelerator (UNILAC) at GSI and was able to accelerate the Ca-ions to around 5 MeV/nucleon. Moreover, the beam had a pulsed structure where a cycle consisted of beam on for 5 ms and then beam off for 15 ms [4, 22].

The cross section for the fusion into element 115 is small, on the scale of picobarns. This is why a relatively high beam intensity and long measuring times are to be preferred. In the

experiment the average number of ^{48}Ca ions that hit the target was $6 \cdot 10^{12}$/s. Due to the high beam intensity the target was mounted on a rotating wheel in order for it not to melt.

Albeit the high beam intensity the production yield and detection of E115 was around two atoms per day. With the high beam intensity comes a lot of background radiation. This complicates matters, as it becomes harder to discriminate the background radiation from the radiation that stems from the SHE decays. The TASCA-separator's task was to sort out the SHE from other reaction products.

3.2 Transfer reaction products

During the beam-target interaction many different product nuclei are created. The interesting ones for this work are the transfer reaction products (TRPs). A transfer reaction is a reaction in which one or more nucleons are transferred between two nuclei. This can be considered a type of a direct reaction in which the particles interact and scatter very fast but it can also be a slower interaction with the formation of a compound nucleus first. TRPs are often a result of grazing collisions, i.e. reactions occurring primarily on the surface of the target nuclei [23]. An example of a transfer reaction between a light beam and a heavier target is illustrated in Figure 3.1.

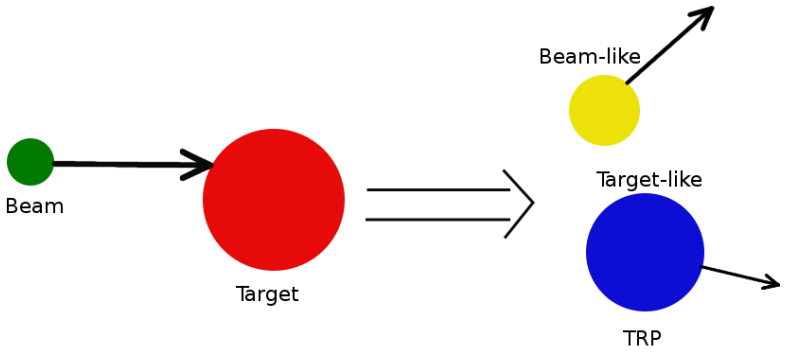

Figure 3.1: Nuclear transfer reaction between a beam ion (green) and a target ion (red). The result of the reaction is a beam-like recoil (yellow) and the target-like transfer reaction product (blue). In the transfer reaction some nucleons from the target nucleus have been transferred to the beam-like recoil particle.

In SHE experiments, the transfer reaction products are much of an inconvenience. This is because they assume similar kinematics, thus also $B\rho$ (described in the next section), and perturbs the detection of the SHE. In the journey to today's SHE experiment many failed experiments has resulted in a lot of transfer reaction product studies. Moreover, these are important to study in order to be able to discriminate these from the desired SHE decays. The production yield in transfer reactions obviously depends on the reaction constituents. An example of the yield in a transfer reaction study can be taken from a time of flight experiment conducted 1996 in Legnaro, Italy, where a beam of ^{40}Ca impinged on a target of ^{124}Sn. In this experiment the transfer of up to 6 neutrons and 6 protons was measured [24].

3.3 TASCA

TASCA is short for TransActinide Separator and Chemistry Apparatus. It is a relatively new gas-filled recoil separator located at GSI which ran its first full scale SHE experiment in 2010 [5]. TASCA can be said to be a classic dipole-quadrupole-quadrupole gas-filled recoil separator. It uses these magnets to separate desired recoiling nuclei, primarily SHEs, to a detector set-up where their properties can be measured.

Charged particles are affected by electric and magnetic fields, as governed by the Lorentz force. The recoiling reaction products that are transmitted through the target in SHE-experiments assume a wide charge-state distribution. Hence, the charge state can vary and this aggravates the separation of the reaction products as the deflection in the magnetic fields are proportional to the charge of the particle. In gas-filled separators, such as TASCA, a dilute gas, e.g. helium, is inserted into the chamber. By collisions with the gas, the reaction products converge to an average charge state and the separation and transmission of wanted products is enhanced [5, 22].

TASCA is sketched in Figure 3.2 and consists of three magnets, one dipole and two quadrupole magnets. The dipole magnet, positioned directly after the target, separates out E115 from other reaction products by adjusting the strength of the magnetic field such that the trajectory of E115 ends up in the TASISpec detector set-up. For charged particles moving in a magnetic field the magnetic rigidity, denoted $B\rho$, is:

$$B\rho = \frac{mv}{q} \tag{3.1}$$

$B\rho$ describes the curvature of the trajectory. For other reaction products the mass and recoil velocity is different. Thus, these assume another trajectory, they are bent off due to different magnetic rigidities and avoids detection. Beam-like particles are comparatively light and assume an increased curvature and end up in a beam dump. The following two quadrupole magnets focus the particles in the horizontal and vertical direction into the focal plane detector, in this case the decay station TASISpec [22].

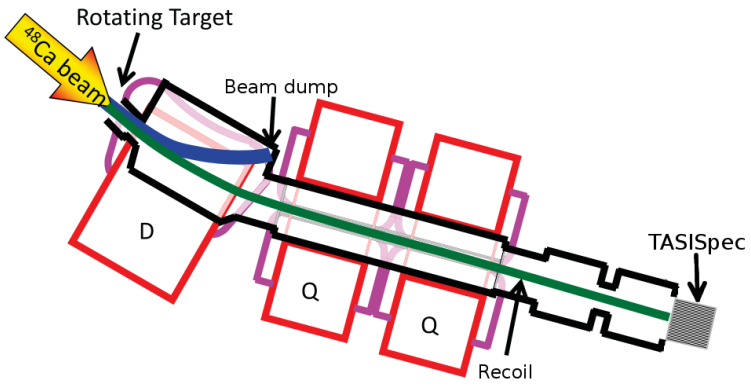

Figure 3.2: Illustration of TASCA with TASISpec (not to scale). The red structures indicates the magnets where D stands for the dipole and Q for the quadrupoles. Recoils enter TASCA after the rotating target. Beam-like particles are bent to a beam dump indicated with a blue trajectory. Typically, heavy TRPs and SHE follow the schematically drawn green trajectory and are implanted to TASISpec at the right side of the figure. Modified figure from Ref. [5].

3.4 TASISpec

The detector set-up employed in the E115 experiment, TASISpec (stands for *TAS*CA in Small *I*mage mode *Spec*troscopy), was developed by the nuclear structure group from Lund University. Today it consists of a combination of DSSSDs and composite HPGe-detectors. The main purpose is to use this highly efficient multi particle-photon coincidence spectroscopic set-up in the study of SHE.

The main constituents of TASISpec are presented in Figure 3.3. Five DSSSDs are set up to create a box-like structure closely surrounded by five composite HPGe detectors mounted as close as possible. The DSSSDs are all 5.8x5.8 cm^2 in area. Except for the implantation detector, which is the one facing the beam and has 32 n- and p-strips, all DSSSDs have 16x16 strips. The implantation detector is 0.52 mm thick while the four other DSSSDs, called the box detectors, are 0.97 mm thick. This results in 1024 pixels, corresponding to an area of about 3.75 mm^2, for the implantation detector and for the box-detectors which are placed upstream (i.e. towards the target) the number of pixels is 256. All the n-strips were processed by analogue electronics whereas the p-strips, which are more appropriate to perform energy extractions from, are on the other hand connected to 60 MHz, 12-bit fast sampling ADCs [4, 25].

The HPGe-detectors are placed as close as possible to the box of five silicon detectors. One CLOVER detector is placed behind each of the box DSSSDs and one CLUSTER detector is placed behind the implantation detector. The signals from the Ge-detectors are processed with commercial 100 MHz 16 bit sampling ADCs from the company Struck Innovative Systeme (SIS). With it came a pulse shape analysis system which for every pulse provided baseline and flat-top values (cf. plateaus in the deconvolution part of the MWD method described in Chapter 4) which, in the offline analysis, could be transformed into an amplitude [4].

3.4.1 Principle

The recoil, say a SHE, is transmitted through TASCA into the implantation DSSSD that faces the beam. Due to the typical recoil energy of the SHE, ~ 30 MeV, they come to a stop about 7 μm into the DSSSD. The implanted SHEs are unstable and decay, in particular E115 α-decays. With a cross-check of the signals from the strips on the p- and n-sides of the detectors it is possible to determine in which pixel the SHE is located. As it decays, signals from the same pixel will be detected and in this way one can keep out signals from other decays in an efficient way. The energies of the α-decays are about 10 MeV. In Si this corresponds to a range of ~ 0.1 mm [26]. The emission of the α-particle can be assumed to be isotropic and this means that there is a significant probability that the α-particle escapes the implantation detector. This is the reason for the box-like DSSSD structure, to capture most of the escaping α-particles.

The p-side of the DSSSD faces the beam and the inside of the box-like structure (cf. Figure 3.3). Recall that the dead layer is a region of the DSSSD which is inactive, i.e. the energy an ionizing particle deposits within the dead layer will be lost. To make up for this, one performs a so called dead-layer correction. By knowing which path the ionizing particle assumes in the detector one can reconstruct its true energy [3].

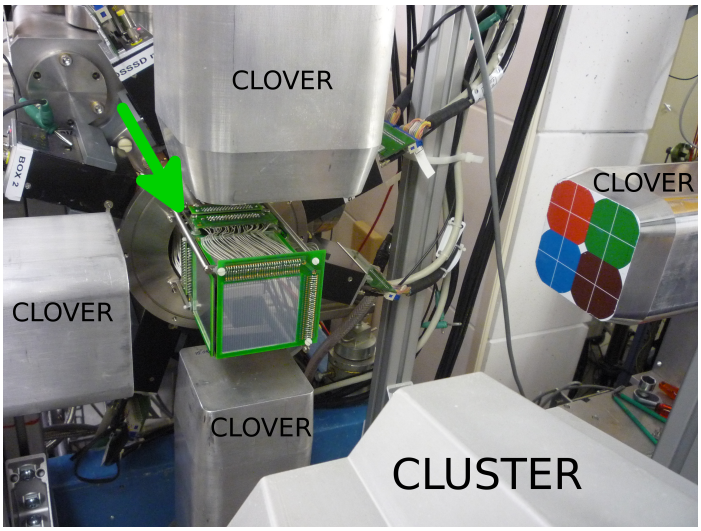

Figure 3.3: TASISpec components. The green-edged box-like structure in the middle of the figure corresponds to the five DSSSDs where the implantation detector is facing the camera. The p-sides are directed towards the inside of the box-like structure. Recoils enter this structure as indicated by the green arrow. In the right part of the figure, the four crystals of a CLOVER detector are indicated with four different colours. The CLOVER detectors goes on the up, bottom, and sides of the silicon detector box. Closest to the camera is the CLUSTER detector, which goes behind the implantation detector [3].

3.4.2 Energy reconstruction

The dead layers in the TASISpec silicon detectors are about 2 μm thick. A dead layer correction is crucial. Escaping α-particles detected in the box-detectors travel through two dead layers and the energy loss is significant and highly dependent on the incident angle. With information of the pixel in the implantation detector and the pixel in the box-DSSSD, the α-particle path can be obtained to a sufficient accuracy, thus also the efficiency of the dead layer thickness. The stopping power as a function of energy of α-particles in silicon is known. With this knowledge the energy loss in the dead layers can be estimated. The total energy of the emitted α-particle can be reconstructed from the energy deposited in the implantation and the box detector together with the energy loss in the dead layers [3].

It is important to note that the energy deposited from an α-decay of an implanted nucleus occurs stems from both the emitted α-particle and the recoiling daughter nucleus. The total kinetic energy emitted in the α-decay is the Q_α-value. The energy of the recoiling daughter nucleus is not usually fully measured due to phonon excitations. A good estimation for it is that about half of the recoil energy is detected [3], i.e.

$$E_{\text{detected}} = E_\alpha + \frac{\Delta E}{2}, \text{ where } \Delta E = Q_\alpha - E_\alpha.$$

where Q_α is calculated through momentum conservation to become:

$$Q_\alpha = E_\alpha \left(1 + \frac{4}{A}\right)$$

3.4.3 Data acquisition

MBS, Multi Branch System, is the name of the data acquisition system (DAQ) which was employed in the E115-experiment. MBS is a GSI locally developed DAQ; as the name suggests, the MBS is intended for data acquisition in a system with more than one branch. A branch refers to different readout routines that can be combined into one, e.g. the combination between VME-based modules connected to the n-strips and FEBEX-based cards connected to the p-strips. The analogue signals from the n-strips were processed with Mesytec ADCs (MADC). MADCs are held in the VME-based modules employed directly after the shapers. The p-side strip preamplifiers are directly connected to fast sampling ADCs. The stored traces were determined to be 4000 samples long which corresponds to about 70 μs for a 60 MHz sampling frequency.

The FEBEX-cards digitise signals continuously from the detectors. When there is a signal with a height larger than a set threshold on the p-side of the implantation detector data from all detectors are stored. For the HPGe-detectors, data was recorded 1 μs before the trigger and 4 μs after. All the data recorded from the p- and n-strips and the HPGe-detectors for this trigger comprise an event, which also includes other parameters from the experimental set-up (e.g. beam status).

3.4.4 Offline data analysis

The raw data from the experiment was stored in listmode-files with a total size of about 3 TB. The offline analysis is split into two parts. The first part is comprised of reading in the raw data and analyse the traces. In the second stage the semi-raw data is calibrated and further processed with algorithms where the analogue times from the VME-modules are aligned to times from the FEBEX-part, a dead layer correction is made and a search for correlated α-decay chains is performed. In this work the silicon DSSSD in TASISpec and the data handling of these is the focus. For complementary analysis of the HPGe-detectors see Ref. [3].

Raw data handling

The raw data handling is performed in GO4. GO4 is based upon ROOT and is a specialisation towards low-to-medium energy nuclear physics and atomic physics experiment handling [27]. In turn ROOT is, as described on their webpage, a C++ based tool which provides support when it comes to data processing, statistical analysis, visualisations and storage [28]. In the GO4-program one event is handled at a time. Firstly the event data is transformed into a desired format. Then depending on whether the data comes from a p- or a n-strip it is treated differently before signal amplitudes and times are compressed to a new ASCII-file. The process is illustrated with the flow-chart in Figure 3.4.

Energy reconstruction and correlation analysis

Tscan, a C-framework, is used for the next step of the offline analysis. Tscan was developed in the 90s' and is handy when it comes to managing spectra in C. The data in the compressed file generated in the previous step is first read in, then data is handled one event at a time and for the n- and p-strip signals the following is done for the energy reconstruction:

- Calibrated energies are calculated with continuous calibration data.

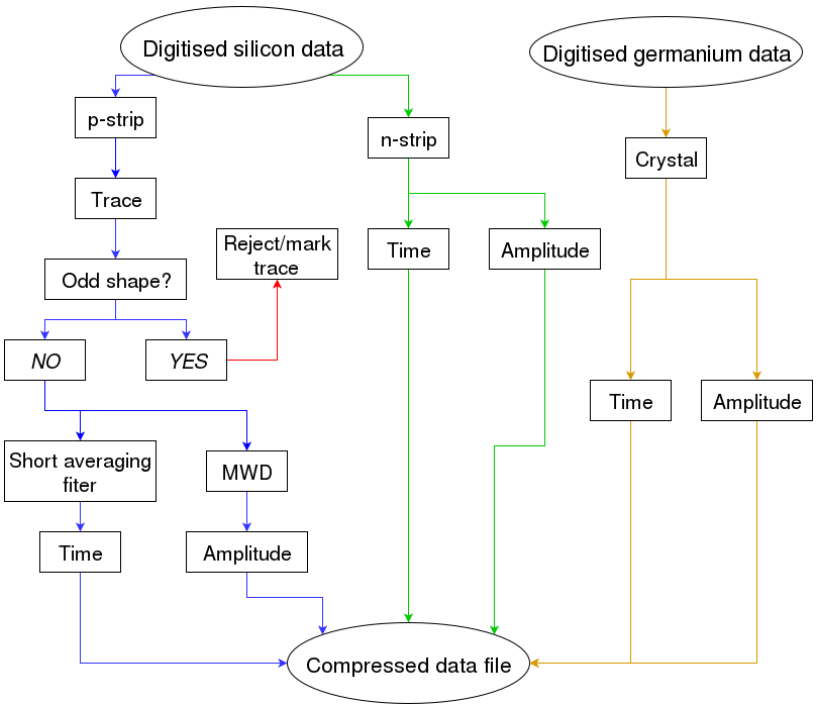

Figure 3.4: A flow chart of the reading and compressing process in the offline data analysis. The traces from the p-strip data are first examined. If a trace assumes an odd shape, i.e. it is a pile-up or just oddly shaped, it is marked and rejected in the further analysis. Otherwise it is run through a short averaging filter to obtain the time of the pulse in the trace and through a moving window deconvolution (MWD) routine to obtain the amplitude of the pulse, see Section 4 for details. From the digitised germanium data, times and indirect amplitudes, baseline and flat-top values, can be read out.

- Analogue times are aligned to trigger times from the p-strips.
- Pixel analysis is performed.
  - If two or more neighbouring strips have energy signals, the energies are summed and added to the strip with the highest original energy.
  - The signals in the p- and n-strips are cross-checked to determine the effective pixel. The energy from the p-side is assigned as the energy when a similar n-side energy is also found.
- A dead-layer correction is made if there are two signals, one in the implantation detector and one in one of the box-DSSSDs, and if these together add up to something α-particle like.

The correlation analysis is based on search criteria, where the energy range of an implant, energy of a first α-particle, energy of a second α-particle (potentially also a third) and limits on the time difference between the implant and the α-particle or the first and second α-particle (potentially also a third), are set. If two subsequent α-decays within a pixel fulfil the energy criteria and the time-difference between the decays fulfils the time criterion it is denoted as an α-α correlation. Similarly, implant-α- and α-α-α-correlations are obtained.

All the measured γ rays are treated simultaneously as the energy reconstruction. If a γ ray is detected within 290-440 ns after the global event trigger they are considered prompt

coincidences. However, the drift time in the Ge-crystals is slightly energy dependent and this was also incorporated for.

Chapter 4

Moving window deconvolution

Moving window deconvolution is a method of pulse shape analysis (PSA), employed to extract energy from digitised preamplifier signals [13, 29–32]. There exist a few different derivations of the MWD method. A more modern approach to the method is presented in [13], [31] and [32]. This is the one given in this section.

The method can be separated into three steps, a deconvolution, a differentiation and an averaging. The complete method, with all these steps, is illustrated in Figure 4.1 for a simulated preamplifier trace with three pulses.

Consider the deconvolution part of the method, cf. Figure 5.19b. The discharge of the capacitor in the preamplifier circuit can to a very good approximation be modeled as an exponentially decaying function with an amplitude A and a decay constant τ [see Equation (2.3)]. The basic idea of the deconvolution part of the method is to exploit this known exponential behaviour. Recall that it is the initial amplitude of the preamplifier pulse that is proportional to the energy deposited by the ionizing particle in the detector.

Assume that a simple preamplifier signal can be described by the following continuous function:

$$P(t) = \begin{cases} Ae^{-\frac{t}{\tau}} & t \geq 0 \\ 0 & t < 0 \end{cases} \tag{4.1}$$

Clearly, this function only assumes the full amplitude, A, at $t = 0$. However, all other values of $P(t)$ for $t > 0$ also contain information of the value of A and therefore it can be good idea to create the function $U(t)$:

$$\begin{aligned} U(t) &= A(t) \\ &= P(t) + A(t) - P(t) \\ &= P(t) + A(t) - A(t)e^{-\frac{t}{\tau}} \\ &= \left[\int_{t=0}^{t} e^{-\frac{t}{\tau}}\, dt = \tau\left(1 - e^{-\frac{t}{\tau}}\right)\right] \\ &= P(t) + \frac{1}{\tau}\int_{t=0}^{t} P(t')\mathrm{dt}' \end{aligned}$$

The digitised preamplifier signal consists of samples $P(t_i)$. In the discrete time domain, $U(t)$ becomes:

$$U(t_i) = P(t_i) + \frac{\Delta t}{\tau}\sum_{t_k=0}^{t_i-1} P(t_k) \tag{4.2}$$

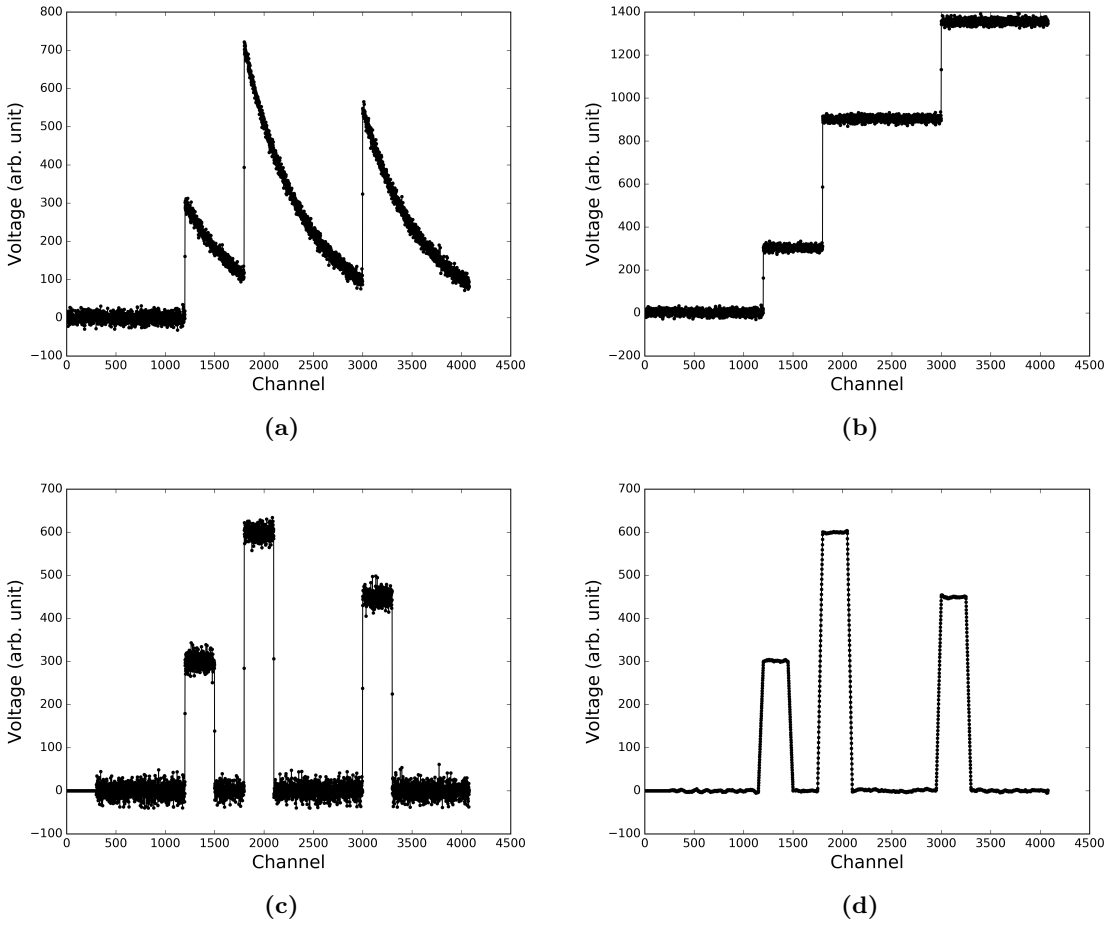

Figure 4.1: (a) A simulated preamplfier signal with three pulses. **(b)** The deconvolution of the simulated signal. The result of the deconvolution is three plateaus. The height of the last plateau corresponds to the sum of the heights of all three pulses. **(c)** The m-step differentiation of the simulated signal ($m = 300$). Three box-like pulses are created. The height of the respective box represents the amplitude of the corresponding pulse. **(d)** The moving window average ($w = 50$) taken of the m-step differentiated signal. This could be interpreted as the MWD-signal.

The integral has been approximated with the Riemann sum and Δt is the sampling time. The right hand side of the equation above is completely known as it consists only of the samples from the preamplifier signal $P(t_i)$. The system can be viewed as in signal processing. In this case the signal entering the preamplifier provides an input $A(t_i)$ describing the induced charge in the detector, which ideally should be described by a step pulse. With a certain transfer function $H(t_i)$, described by the intrinsic properties of the preamplifier, an output $P(t_i)$ is created. The output is obtained through the deconvolution of the input and the transfer function:

$$P(t_i) = H(t_i) * A(t_i) \tag{4.3}$$

The amplitude of $P(t_i)$, is determined by $A(t_i)$ and it is in turn obtained through a deconvolution of the transfer function and the output. This is the reason why this part of the method is called deconvolution. After the deconvolution the signal is transformed into a step pulse as can be seen in Figure 4.1c. The deconvolution removes the exponential

behaviour and the result is a plateau with constant height.

If the preamplifier signal is a perfect exponential function then $U(t_i)$ becomes a step signal, a Heaviside step function. Obviously, this is not the case for a physical real signal. A real signal typically contains electronic noise. $U(t_i)$ allows to obtain an accurate estimate of the value of A based on several measurements.

It is important to note that in the deconvolution it is assumed that there is no off-set to the preamplifier signal [cf. Equation (4.1)]. Therefore, to perform the deconvolution it is necessary to remove the off-set, i.e. setting the baseline to zero.

The length of the exponential decay of the preamplifier signal is in theory ∞, although not in practice. Nonetheless, the baseline will rise for subsequent pulses. To restore the baseline values, the step-pulse is shortened with an m-step differentiation of $U(t_i)$:

$$M(t_i) = \nabla_m U(t_i) = U(t_i) - U(t_{i-m}) \tag{4.4}$$

The differentiation is the second part of the method. The effect of the differentiation on $U(t_i)$ obviously depends on the choice of m. For samples t_i before the arrival of the pulse, $M(t_i)$ is approximately zero. If m is set to be sufficiently large (significantly larger than the rise time of the pulse), then the signal $U(t_i)$ will become a box-like pulse. For samples t_i in the beginning of the deconvolved pulse $U(t_i)$, $M(t_i)$ will steadily rise until it becomes approximately constant. As the m-shifted part, $U(t_{i-m})$ reaches the pulse, it will assume a value similar to that of the unshifted $U(t_i)$, and $M(t_i)$ will approach zero again. As illustrated in Figure 4.1c, in the situation of a pile-up pulse, the m-step differentiation will be able to separate the pulses if m is chosen to a value smaller than the time separation of the pulses.

Ideally, the amplitude of the box-like pulse should be computed as the mean of infinitely many samples to remove the noise perturbation. Even though there obviously does not exist infinitely many samples, taking the mean of many should help to eliminate the noise and improve the amplitude measurement. The mean is obtained using the moving window average method. The moving average method applied to $M(t_i)$ gives:

$$MA(t_i) = \frac{M(t_i) + M(t_{i+1}) + ... + M(t_{i+w})}{w} \tag{4.5}$$

Here w indicates the length of the window, i.e. the width of the range of which is to be taken an average of. The moving average of a box-like pulse results in a trapezoidal pulse (if $w < m$). This is the reason to why the complete method is sometimes referred to as a trapezoidal filter.

Throughout the differentiation and the moving average, the height of the step pulse with respect to the baseline (proportional to the energy) has not been altered. The last step in the moving deconvolution method is to extract the height of the trapezoid. The position on the flat top of the trapezoid for which this is done is preferably chosen to be after the signal has stabilised, where the overshoot has diminished [31].

The choice of the parameters τ, m and w deserves a further comment. τ is preferably determined through a linear regression on $y = Ae^{-\frac{t}{\tau}}$ to the sum of many traces. Taking the sum of traces, the exponential shape is not altered, while the noise fluctuations in the signals will even out to a large extent. The other parameters, m and w, are usually determined through some hands-on testing on the traces which are to be examined. A more detailed description of how to choose τ, m and w is given in Section 5.3.

Chapter 5

Pile-up trace analysis routine

Method development and description

In this chapter the routine which extracts amplitude and time for pulses in pile-up preamplifier traces in the E115 experiment is described. In the development of the method, characteristics of viable traces which include for instance rise times and decay times, were important. Viable are those traces which reflect a normal behaviour of a preamplifier. This subject begins the chapter.

Undesired pulses of different types appeared throughout the experiment and to automatically discriminate those from the viable ones is somewhat of a challenge. A filtering method was developed to only extract proper physical events and their characteristics. The second part of this chapter handles this filter and the extraction of the times of the pulses which was done simultaneously.

The well established method to extract amplitudes from digitised preamplifier traces, Moving Window Deconvolution (MWD), was studied thoroughly to obtain a handle feeling for the basics of energy extraction. In the last part of the section it is described how the MWD-method has been deployed to treat viable traces of any kind, but a special focus lies on pile-up traces. The use of the different steps of the MWD-method, deconvolution, differentiation and averaging, are carefully described in the last part of the chapter.

5.1 Trace characterisation

In order to characterise viable preamplifier traces, i.e. standard single-pulse traces, pile-up traces and saturated traces, a batch of experimental traces was selected from one data file of the E115 experiment. From this batch, important features such as rise times, decay times and differentiated traces, were studied. Especially the start of the rising edge and the falling edge of a pulse were considered as important characteristics since these were to be main elements in the process of determining the parameters in the MWD-method. The characteristics of a standard experimental double-pulse trace are illustrated in Figure 5.1.

From studies of several traces with different heights the following characteristics of a pulse were established:

- The rising edge can be distinguished as around 5 subsequent relatively large samples in the differentiated trace following at least one that exceeds a value of 60 (cf. Figure

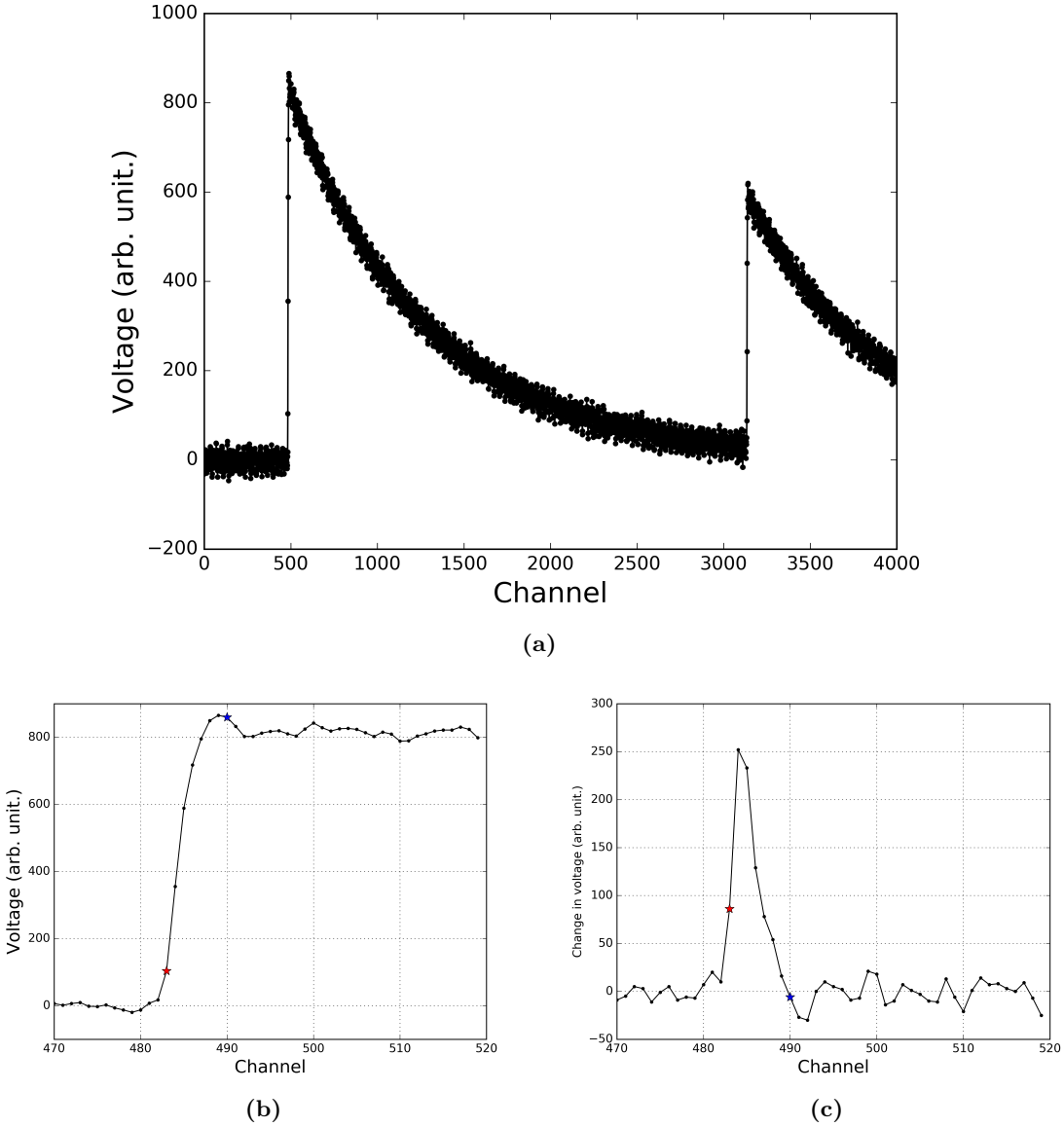

(a) **(b)** **(c)**

Figure 5.1: (a) A double-pulse trace obtained from the E115 experiment. The noise is quite noticeable. **(b)** The first pulse in the double-pulse trace in (a) zoomed in. **(c)** 1-step differentiation of the first pulse in the double-pulse trace. The red and blue stars indicate the channel at which the rising edge of the pulse begins and the falling edge of the pulse starts, respectively. Deduced from (b) is that the rising edge consists of about 5 samples and a clear overshoot is present. From (c) it is easy to distinguish the beginning of the pulse as large values of the 1-step derivative. The start of the falling edge can be interpreted as a differentiated channel at which the derivative has returned to about zero (see text for details).

5.1c). In this work the sample at which the rising edge is initiated is denoted t_{rise}.

- The start of the falling edge is trickier to distinguish, due to the noise and natural fluctuations that are present in the trace. It can be determined as a channel after the differentiated trace has returned to below a value of 10. In this work the sample at

which the falling edge starts is denoted t_{fall}.

These features are used as a part of the filtering method to determine t_{rise} and t_{fall}. This is described in the next section.

One of the main purposes of the E115 experiment was to detect α-decay chains originating from element 115. To do this it was important that the preamplifiers and the ADCs had a sensitivity to distinguish the α-decay energies and the fast sampling ADCs had to cover a specific range. The upper limit of the ADCs were set to about 15-18 MeV. Beam implants and fission decays have energies above the upper limit of the ADC. In the E115 experiment a 12-bit ADC was employed and thus the highest value it assumes is $2^{12} - 1 = 4095$, as the first value is 0. Events with energies higher than 18 MeV occur, so called saturated events were recorded as illustrated in Figure 5.2.

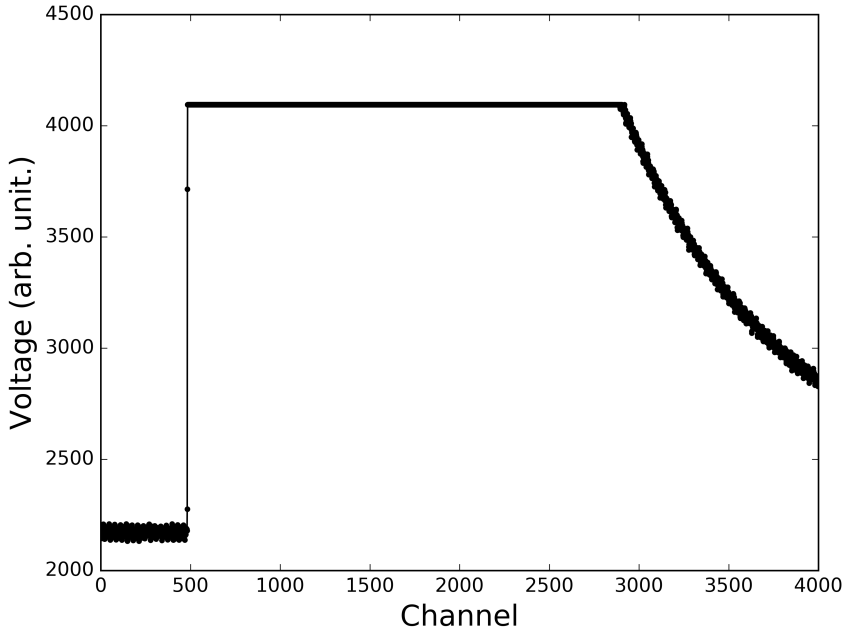

Figure 5.2: Saturated trace. As the preamplifier output exceeds the digitiser upper limit, the ADC keeps the value to 4095. Due to that pulses with negative polarities can also be measured, the baseline is located at $\sim 4095/2$. This trace has not been baseline restored (note the offset).

Saturated traces also fall in the scope of this work as α-decay pile-ups can result in large outputs from the preamplifier. Furthermore, short-lived transfer reaction products that are implanted in the detector and then decay can also result in saturated traces.

A regular saturated trace is presented in Figure 5.2. A general feature of the saturated trace is that they assume a very short rise time (only over 1 sample). The recorded value at which the ADC is saturated was in reality the values 4094 or 4095. The treatment of a pile-up saturated trace is described in the next section and illustrated in Figure 5.8.

Unexpected large noise and oddly shaped pulses sometimes are present in the traces. Examples of four non-standard traces are illustrated in Figure 5.3.

The difficulty with the traces in Figure 5.3 is that all of them assume locally similar properties to viable traces while at the same time they do not represent physically meaningful

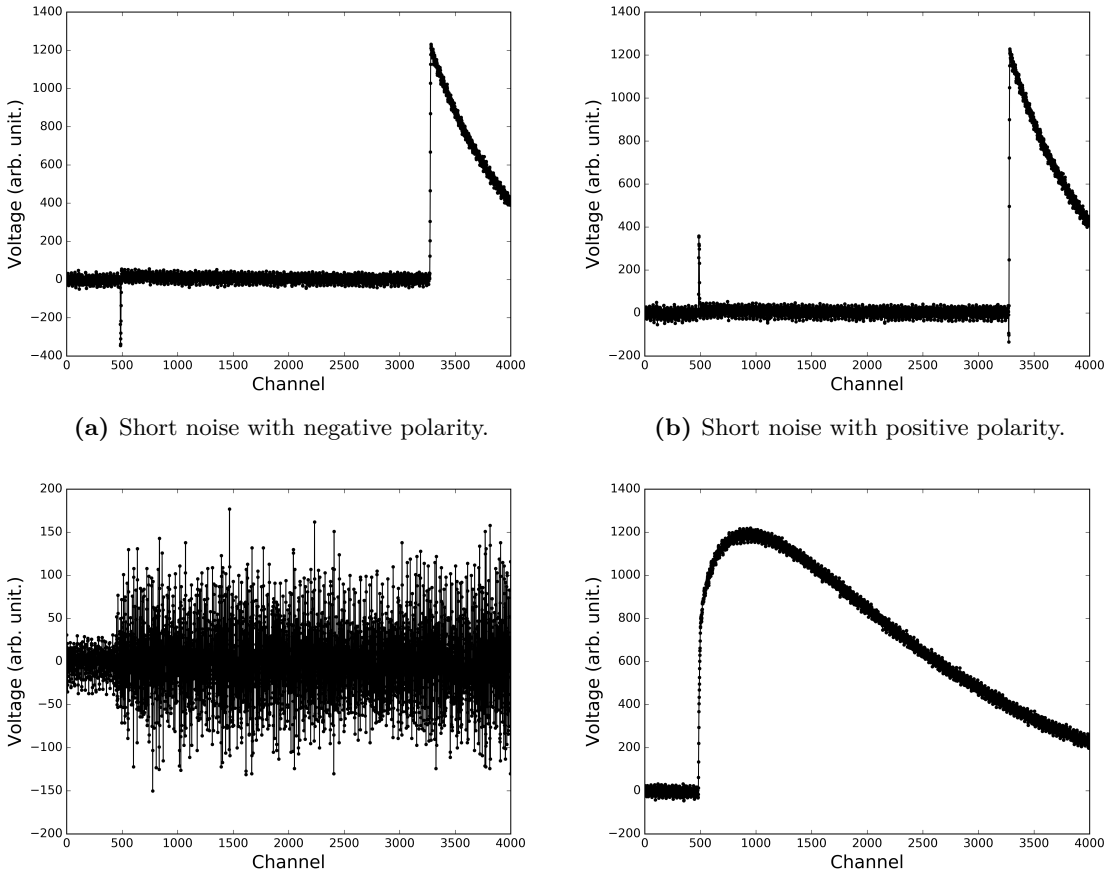

(a) Short noise with negative polarity.

(b) Short noise with positive polarity.

(c) Large noise train.

(d) *smeared* pulse.

Figure 5.3: Unexpected and oddly shaped traces. These traces have similar properties to the viable traces and the analysis routine needs to be able to tell them apart.

pulses. The *smeared* pulses need to be excluded since the proportionality towards induced charge in the detector is not valid. In the assumption of the proportionality a very fast rise time is assumed (see Section 2.2.1). The short noise pulses do not represent a proper physical event since the decay is too fast, the capacitor in the preamplifier cannot be discharged within only about 6-7 samples (about 100 ns) as is the case with the short noise, regardless of the polarity.

Why do the undesired pulses occur? To improve the complete detector set-up, with the detectors, preamplifiers and digitisers it is useful to clarify the origin of these pulses. To achieve this, an indicator was set to stop the programme when an event containing a non-standard pulse was registered. Recall that an event is comprised of digitised traces from all preamplifiers (96) as only for those above a certain threshold, the trigger is activated. Figures 5.4 and 5.5 illustrate events in which short noise and *smeared* pulses should not occur.

Also, pulses with odd exponential decays were found and could be assigned to cases assuming the characteristic presented in Figure 5.6.

From the study of physically meaningful traces, important characteristics of the pulses

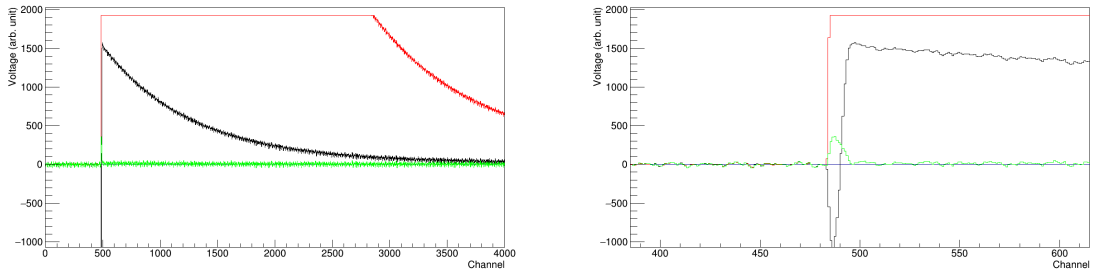

(a) **(b)**

Figure 5.4: **(a)** Full event with short noise of both polarities present. The three colours represents signals superimposed from three adjacent strips in the implantation detector. **(b)** The figure in (a) zoomed in around channel 500. From this figure the structure of the short noise is evident. Short noise pulses were conclusively observed in neighbouring channels to high saturated pulse.

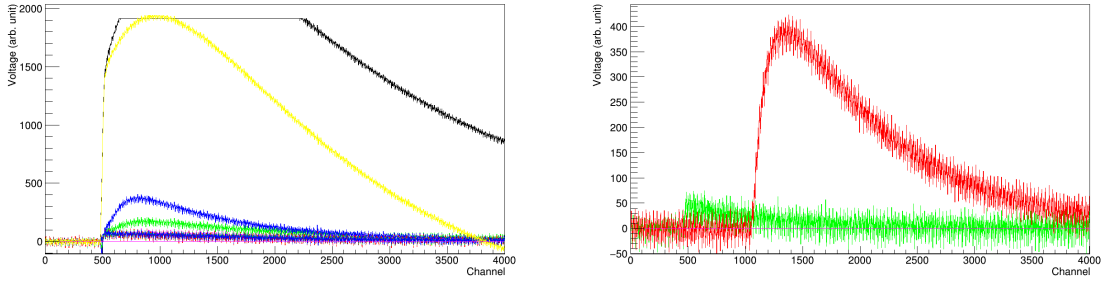

(a) **(b)**

Figure 5.5: **(a)** Full event with *smeared* pulses. The different colours represent superimposed traces from the different strips of the implantation detector. Here, all strips have a signal. *smeared* pulses were often found in events with a high saturated pulse and a high multiplicity of traces. **(b)** Full event with a *smeared* pulse and where only two strips had a signal. The *smeared* pulses could also be found in what appears to be normal events.

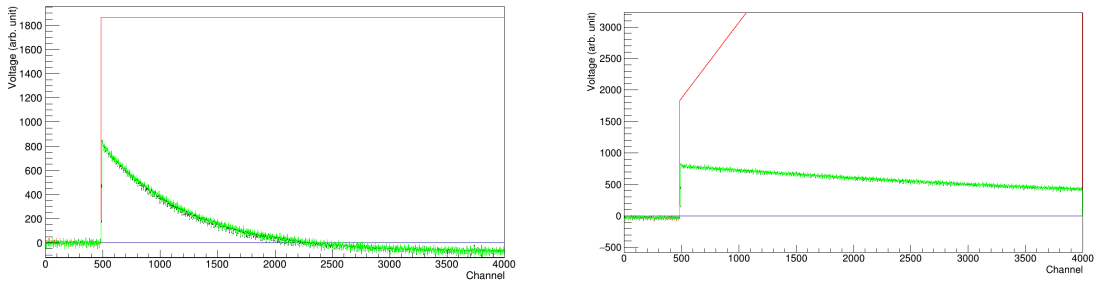

(a) **(b)**

Figure 5.6: **(a)** Traces from three adjacent strips in the implantation detector (strip 12 black, strip 13 red and strip 14 green). **(b)** Deconvolution of the traces in (a). Note the non-existing plateaus after the deconvolution step (cf. Figure 4.1b).

could be established which would come to use in the application of the MWD method. Different oddly shaped traces were identified. These could almost exclusively be found in

events where many p-strips had signals. Hence, the number of p-strips with signals could potentially function as a valid condition to reject the oddly shaped traces for further analysis.

5.2 Filtering and time extraction

To determine the characteristics of a trace and to exclude the undesired pulses, a filtering method was developed. Proceeding from the features described in the beginning of 5.1 and after some hands-on testing, t_{rise}, which is assigned to the time of a pulse, and t_{fall} were determined. The basic principle of the filter was a counting of the number of pulses in a trace. The trace samples are iterated through in a loop and, the design of the method goes as follows:

1. If the 1-step differentiated trace assumes a value larger than 60 a pulse-trigger is switched ON.

2. If the pulse-trigger is ON and the 1-step differentiated trace assumes a value smaller than 10, the pulse-trigger is switched OFF.

After the end of the loop the number of ON-OFF switches is calculated. The obtained number represents the number of pulses in the trace. The threshold should be set as low as possible and it was determined as 60 because otherwise noisy traces were extracted.

The so called *short noise* pulses had a rise time typically over two samples. By including a condition that the number of samples between the ON and OFF switch had to exceed 2 samples, many of the *short noise* traces could be identified. However, to avoid miss-identifying the saturated traces which also had short rise times, the short pulse also needed to have a height below 800. To be able to remove all *short noise*s with a positive polarity it was necessary to include the condition that the height of the pulse where the falling edge starts subtracted with the height of the trace 10 samples forward in time should be smaller than 100. The large noise train is simply noise with a large magnitude. To remove such traces, the total average of the trace from t_{rise} to the end of the trace needed to exceed 30.

Concerning the *short noise* with negative polarity, all of these were removed by implementing an indicator when two subsequent values of the 1-step derivative were lower than -60 and -20. The duration of the *short noise* pulses were typically less than 10 samples. The following 15 samples after the negative *short noise* indicator had been activated, the pulse-trigger could not be switched ON.

The *smeared* pulses were particularly problematic as they assumed most of the similar features of proper pulses. The most protruding characteristic of the *smeared* pulses considered, was its very long rise time. However, to study only the rise time was deemed too inconclusive. This is because it was difficult to determine the end of the rising edge of a pulse and the rising edge of a *smeared* pulse assumes similar characteristics of the rise of a pile-up trace with two pulses with a small time difference (cf. Figure 5.19a). After some hands on testing it was concluded that the most accurate way to distinguish whether a pulse was *smeared* was to study the differentiation of the deconvolved trace. The implemented method is illustrated in Figure 5.7.

The method to discriminate *smeared* pulses is based on counting the samples that exceed a threshold set to the value 70 in a 20-step differentiated deconvolved trace. The threshold value was set to 70 in order to be above the noise in the differentiated deconvolved trace

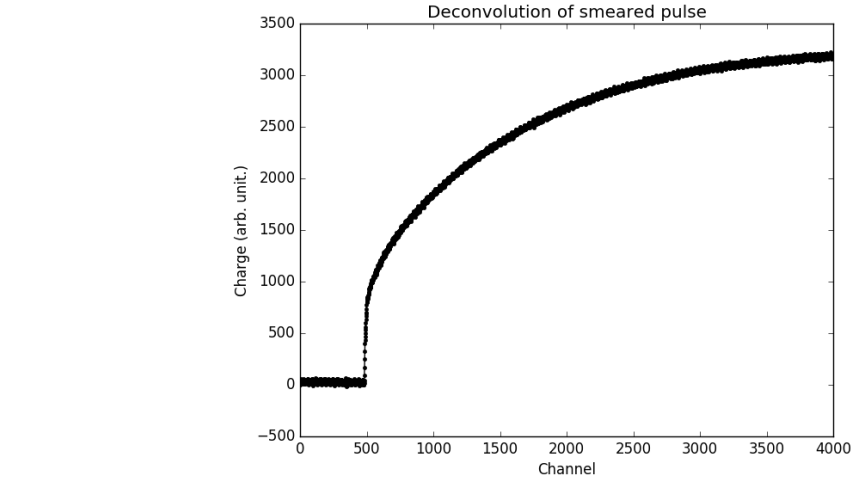

(a)

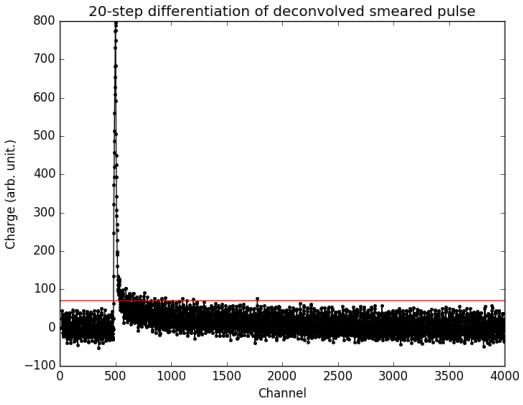

(b)

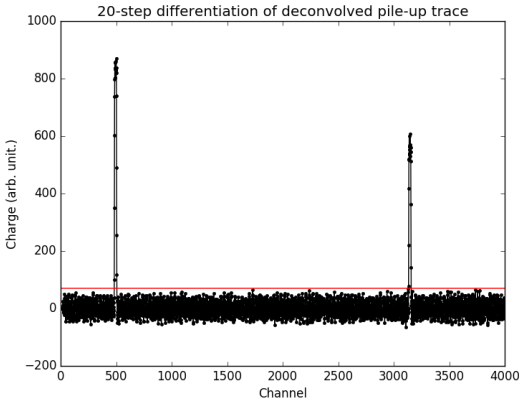

(c)

Figure 5.7: (a) Deconvolution of the *smeared* pulse presented in Figure 5.3d. **(b)** 20-step differentiation of the deconvolved *smeared* pulse in (a). **(c)** 20-step differentiation of the deconvolved pile-up trace in Figure 5.1. The red line in (b) and (c) represents a threshold at value 70. To distinguish the *smeared* pulses, the number of samples in the differentiated deconvolved traces above the threshold is counted. In (b) this number is 110, while in (c) it is 47. The limit for which a pulse is accounted as *smeared* was set to 80. More details in text.

which typically assumed a maximum of around the value 50. With the hands-on testing, a limit on the number of samples exceeding the threshold was set to 80. With a value of 80, also triple-pulse traces are avoided. One could think that it would be sufficient to merely study a differentiated trace. However, the total rise time of a double-pulse trace is similar to the rise time of a *smeared* pulse and this aggravates this approach. Furthermore, the method to extract t_{rise} and t_{fall} actually removes the majority of the *smeared* pulses. This is because the one-step derivative of a *smeared* pulse does usually not assume values above 60 at all.

In the filtering, simultaneously as the number of pulses was counted with the number of ON-OFF switches, t_{rise} and t_{fall} were determined. t_{rise} for a pulse was determined as

the channel when the pulse trigger was switched ON, unless the preceding 1-step derivative exceeded the value 35. If this occurred, t_{rise} was assigned to the channel before the pulse trigger was switched ON in order to really obtain the first sample on the rising edge. t_{fall} for a pulse was then determined, when the pulse trigger was ON, as the first channel which the 1-step derivative was below the value 5. This was unless the subsequent 1-step derivative was less than the value 30. In that case it was assigned to the subsequent channel to avoid a possible overshoot present in the trace.

The conditions set in the filter to determine t_{rise} and t_{fall}, were carefully tuned such that the obtained values almost exclusively coincided with the correct ones. This was satisfying as these were crucial in the process of setting the parameters in the MWD algorithm, m and w, see Section 5.3.

In the existing routine, the number of samples that assumed the value of 4095 were counted. From this number, the amplitude of the saturated pulse could be determined with an extrapolation (see Section 5.3). As the ADC-value of a saturated trace was concluded to actually assume, besides the value of 4095, also 4094, the existing routine treated some of the saturated traces in an incorrect way.

The saturated traces in this work were preferably not analysed in a similar way as the existing routine and this was mainly because two subsequent pulses in a trace could reach saturation. In this work, for pulses that reached saturation, t_{rise} and t_{fall} were determined in the same way as described earlier. By itself t_{fall} cannot be considered a very important feature of the saturated pulses. Instead the channel at which a saturated pulse returned to values below the upper limit of the ADC, denoted t_{sat}, and for the number of samples it was saturated, denoted sat_{dur}, were relevant characteristics. With t_{sat} and sat_{dur} the projected height of a saturated pulse could be obtained with an extrapolation (see Section 5.3.1).

With a similar approach as with t_{rise} and t_{fall}, t_{sat} was determined. As the trace (which had not been baseline restored) assumed the value 4095 a trigger was switched ON. If the trigger was ON and the value of the trace returned below 4090 the trigger was switched OFF and this channel were assigned as t_{sat}. Simultaneously, sat_{dur} was determined as $t_{sat} - t_{fall}$. Due to the noise in the signal, the OFF-switch limit was set to 4090 instead of 4094. Furthermore, in some cases, the noise was specifically troublesome as depicted in Figure 5.8.

From the inset in Figure 5.8 it can be seen that due to the presence of electronic noise, the pulse alternates between saturation and no saturation. It is desired to extract t_{sat} as the channel indicated with the cyan square. To ensure this, a condition between the end of one saturation and the start of another saturation needed to be separated with at least 10 channels. Note that because two saturated pulses might occur consecutively it is not sufficient to naively count the number of samples that assume the value 4094 or 4095.

Through a detailed study on one of the E115-experiment data files, it was clear that the method failed to identify a few pile-up traces. To these belonged double-pulse traces which reflected the event wherein one α-particle deposited its full energy in the implantation detector and one escaping α-particle which only deposited a fraction of its energy in the implantation detector and the rest in a box detector (see Figure 5.9). This implies that some pile-up trace data were not extracted with the routine and this can be considered as the biggest limitation of the routine.

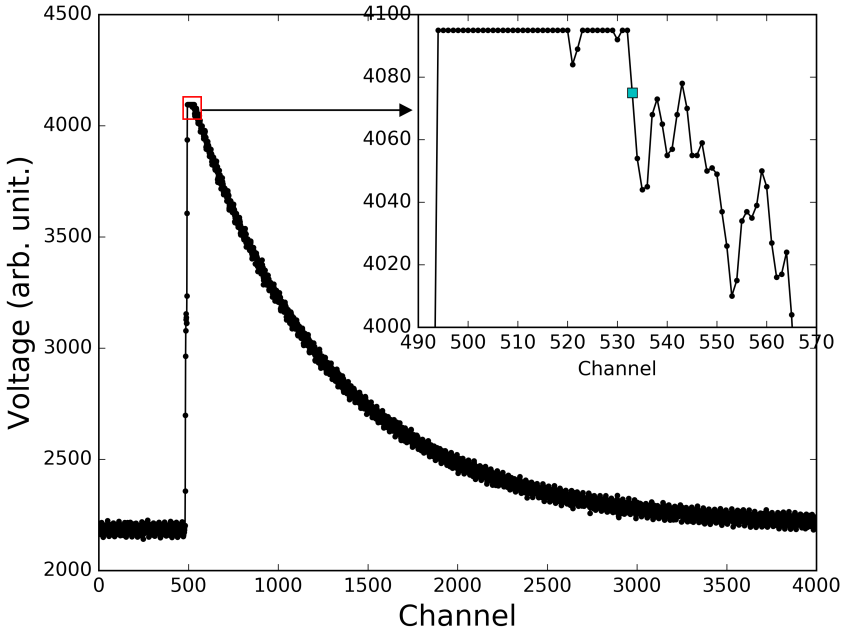

Figure 5.8: Pile-up trace which reaches saturation. The inset in the top right corner of the figure presents the saturation part of the trace zoomed in. From this plot it is evident that the trace alternates between saturation and no saturation, twice. The cyan square indicates the channel at which the saturation can be safely assumed to be over.

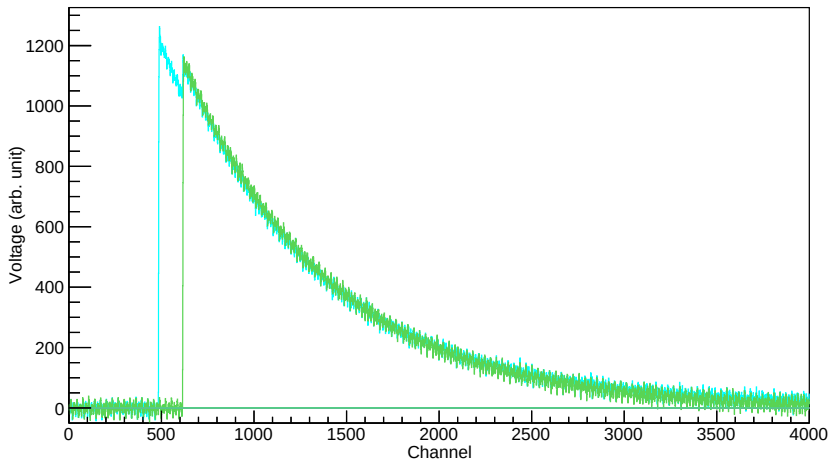

Figure 5.9: An example of a pile-up trace which the filtering method failed to identify. The cyan and green lines represent signals in the implantation detector and one of the box detectors, respectively. The filtering method assigned the number of pulses in the cyan trace to only 1.

5.3 Amplitude extraction with the MWD method

Once the pile-up traces had been identified and the times have been obtained from the traces, the next phase comprises on how to implement a general method for amplitude extraction of pile-up traces. This was achieved with an extension of the MWD method, which was thoroughly walked through in chapter 4.

To start off, the traces were normalised to a baseline value as there always existed an offset (cf. Figure 5.2). This was important because the deconvolution part of the method otherwise was not possible [see Equation (4.1)], but also since the output voltage could vary between different preamplifiers and digitisers and also be time dependent. In the experiment the traces were recorded such that the pulse occurred at about sample 500. Therefore, a baseline value was calculated as the average of the first 400 digitised samples. The restoration was then accomplished through a subtraction of the obtained baseline value.

5.3.1 Deconvolution and τ estimation

Essential to the deconvolution is the estimation of the exponential decay constant τ. The better the estimate, the more flattened plateau should be obtained. In theory the decay of the preamplifier trace is a perfect exponential. However, this was not the case in reality (see Figure 5.11). For pile-up traces deconvolution is particularly important as any subsequent pulse is "riding" on a deconvolved preceding pulse. This results in an incorrect extracted amplitude which is illustrated in Figure 5.10.

If the deconvolution is not correct this will result in a changing height of the plateau and the height of a subsequent pulse will be affected. In the existing MWD routine for the E115 experiment the estimation of τ was made on the basis of the first 390 samples after the start of the decay of the pulse. The reason why no more samples were included was that the fit worsened and it was not really needed. This estimate had the consequence on the deconvolution that the plateau was constant for only about those 390 samples. However, this was not a problem at the time since only single-pulse traces were considered. Computing the height as an average of over 320 samples was sufficient. For the newly developed amplitude estimation routine for pile-up pulses it was concluded that a new estimate of τ was needed.

The exponential decay constant, τ, is mainly determined by the properties of the preamplifier. In the case of the E115 experiment 96 different preamplifiers were employed to record traces from the 96 p-strips. One estimate of τ was performed for each preamplifier; as every preamplifier is slightly different from the other.

As briefly mentioned at the end of Chapter 4, to estimate τ as accurate as possible, an exponential $y = Ae^{-\frac{t}{\tau}}$ is fitted to the sum of many traces. From now on, the sum of many traces from one preamplifier is denoted Σ. A simple linear regression fit is performed to the logarithm of the sum of many traces and with the estimated slope $\hat{k}$, the estimate of τ can then be made as follows.

$$\Sigma = Ae^{-\frac{t}{\tau}} \Rightarrow \ln \Sigma = \ln A - \frac{1}{\tau}t \Leftrightarrow \widehat{\ln \Sigma} = \widehat{\ln A} + \hat{k}t \tag{5.1}$$

Here the hatted variables indicate that they are estimates (or fits). Hence, the estimate of τ can be obtained as $-\frac{1}{\hat{k}}$ or as:

$$\tau = -\frac{1}{\frac{\widehat{\partial \ln \Sigma}}{\partial t}} \tag{5.2}$$

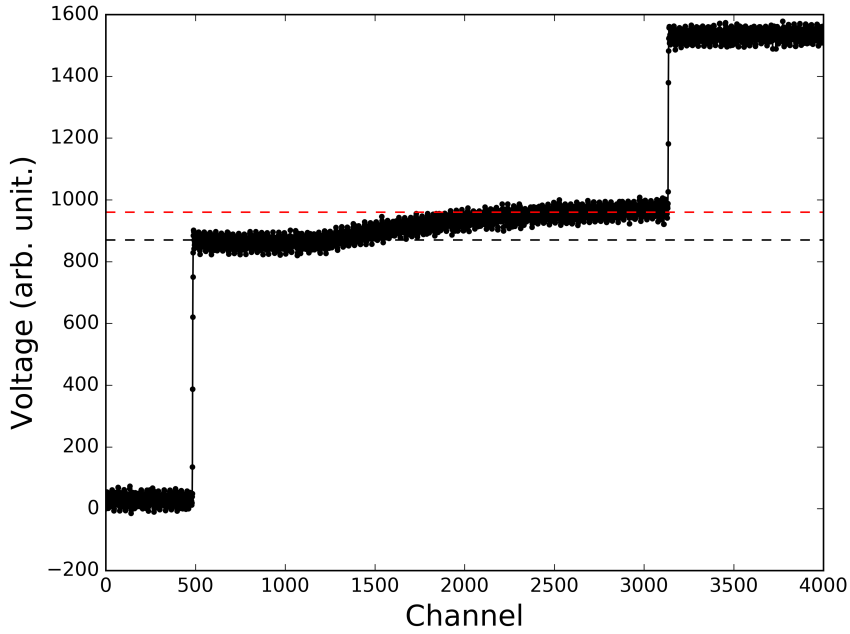

Figure 5.10: Deconvolution of the double-pulse trace shown in Figure 5.1a (the deconvolution has been modified for enhanced effect). The dashed black line indicates the original height of the first pulse and the dashed red line indicates the height of the deconvolution at the rise of the subsequent pulse. It is observed that due to a complex behaviour of the preamplifier decay there is not a constant plateau present between the pulses. Furthermore, it is also evident that the height at the end of the trace does not correspond to the sum of the individual pulses.

To study the estimate of τ, a batch of about 30000 single-pulse viable traces were acquired from a data file from the E115 experiment. To start off, a linear fit was performed to the first 390 samples after the start of the decay of the pulse. The start of the decay of the pulses could vary a little, however almost all pulses started before channel 510 and thus this was chosen as the lower limit for the procedure. The obtained linear fit is shown in Figure 5.11.

As can be seen from Figure 5.11, $\ln \Sigma$ does not have a linear behaviour over the length of the trace. To correct for this behaviour the full trace of $\ln \Sigma$ was fitted to different polynomials. The best fit was obtained for a fourth degree polynomial $a + bt + ct^4$. An example of the result of this fit is presented in Figure 5.12.

Although the fourth degree polynomial fit looks very good, it was doubtful to rule out the linear fit for channels 510-900. This was further studied by a comparison of the sum of the squared errors in both fits for channel 510-900 for all 32 preamplifiers in the implantation detector. The result is presented in Figure 5.13.

Based on Figure 5.13 it was concluded that it is advantageous to split the fit into two parts, first a linear fit and then the polynomial fit. To verify that the proper end of the range for the linear fit was in fact 900 a test was performed. The mean of the squared errors for the linear fit was computed for different ranges, 510-600, 510-610 ... 510-1500. In order to compare the different values the sum of the squared error was normalised with respect to the number of samples used in the fit. The result of this range evaluation is shown in

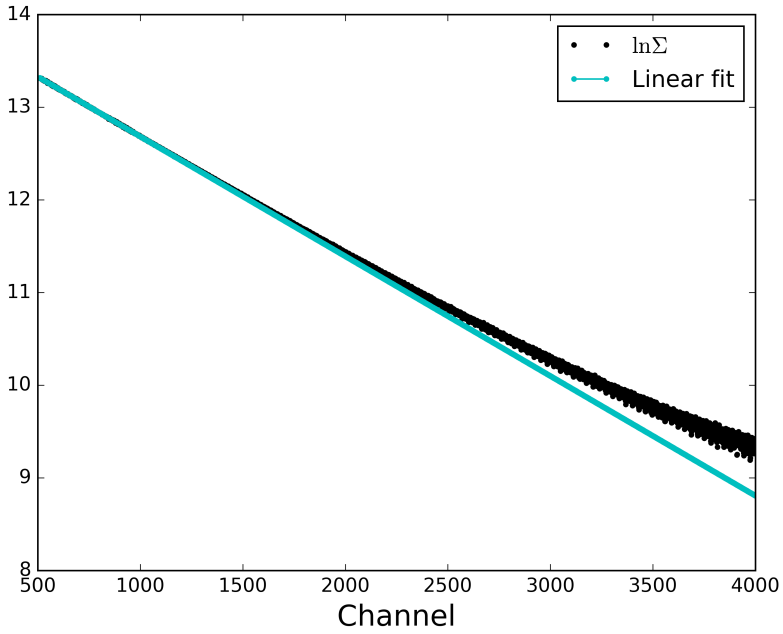

Figure 5.11: Linear fit (cyan) based on the range channel 510-900 to the sum trace, $\ln \Sigma$, (black dots) for a given preamplifier.

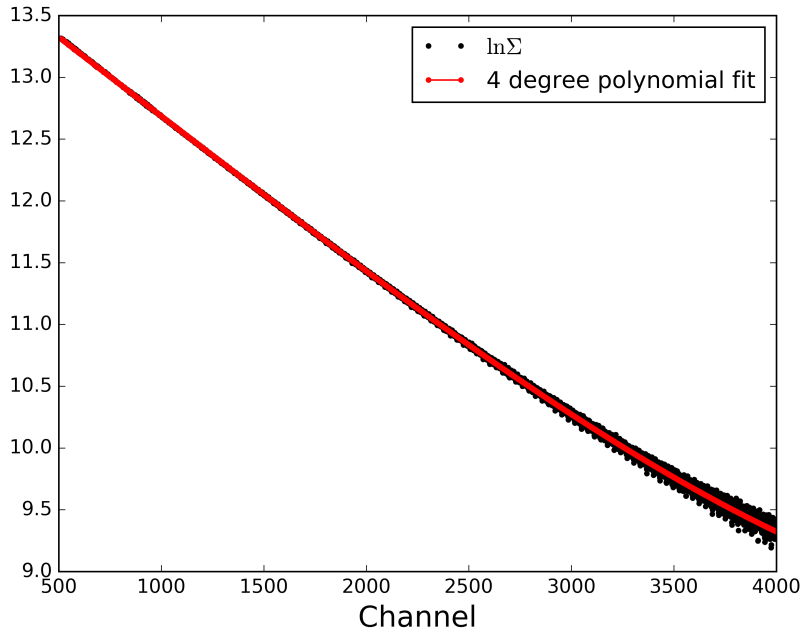

Figure 5.12: Fourth degree polynomial fit (red) to the channel range 510-4000 of $\ln \Sigma$ (black dots) for a given preamplifier.

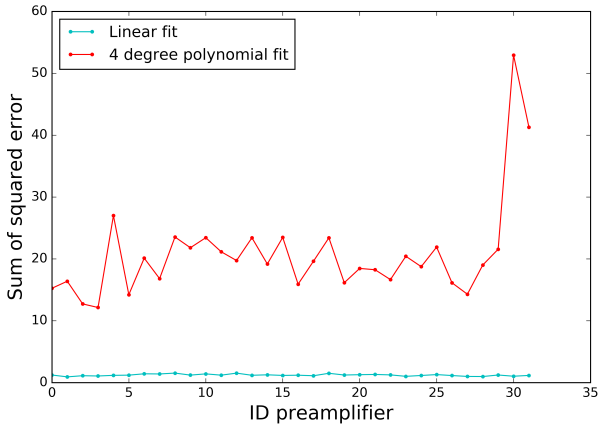

Figure 5.13: Sum of the squared errors for both fits on channels 510-900 for all 32 preamplifiers in the implantation detector. The linear fit is in cyan and the fourth degree polynomial fit is in red. The values for the two last preamplifiers in the fourth degree polynomial fit stand out. This is likely due to low statistics.

Figure 5.14.

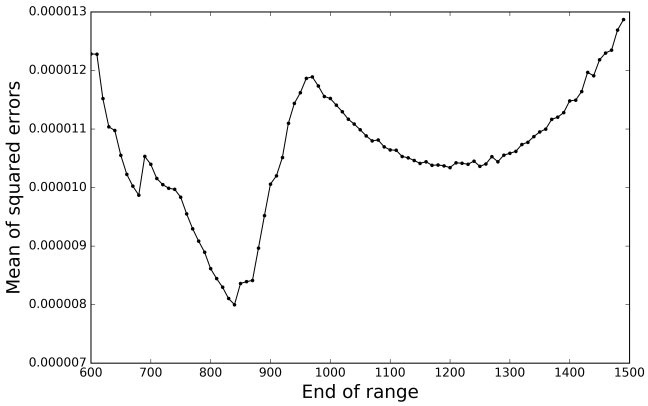

Figure 5.14: Mean of the squared error for the linear fit to $\ln \Sigma$ computed for different ranges starting from channel 510 for a given preamplifier. A large increase in the error is noticeable near channel 900 which indicates that a change in the exponential behaviour of Σ occurs.

It is rather clear from Figure 5.14 that the fit works best up to channels 800-900. A similar behaviour was found for all preamplifiers. It was concluded that the linear fit should be used for channels between 510 to 900 and the fourth degree polynomial fit for channels 900 to 4000. The estimate of τ was computed as in Equation (5.2). The backwards 1-step derivative was used as the derivative. The resulting values of τ are presented in Figure 5.15. It can be noted from the figure that there is a small gap at the transition between the two fits. This gap has a negligible effect on the deconvolution.

As a verification of the new estimate of τ, the deconvolution with the old estimate of τ and the new estimate of τ were computed for Σ for a given preamplifier, see Figure 5.16.

Pile-up traces also demand a slightly different deconvolution. In Figure 5.15 the estimate of τ is presented as a function of channel in the trace. Though, fully functional, this

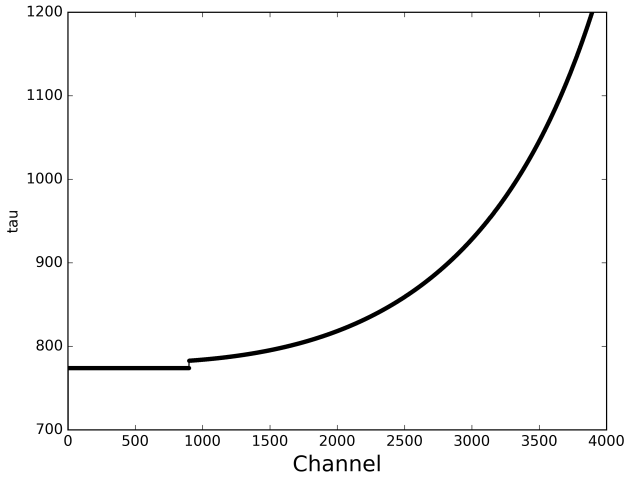

Figure 5.15: Improved estimate of τ as a function of channel for a given preamplifier. The simple linear estimate governs the first 900 channels while the rest is governed by the improved estimate based on the fourth degree polynomial fit.

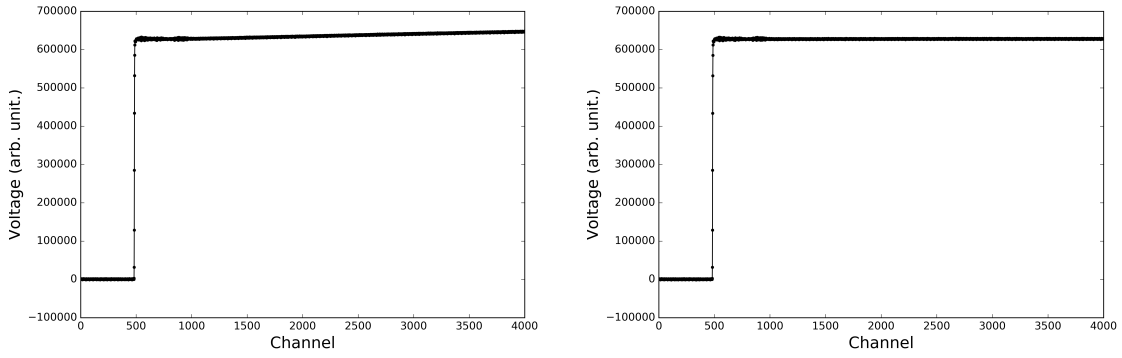

(a) **(b)**

Figure 5.16: **(a)** Deconvolution of Σ with the original simple linear estimate of τ. **(b)** Deconvolution of Σ with the improved estimate of τ.

representation of τ holds true for single-pulse traces. What is depicted in reality is the τ after the occurrence of a pulse. What occurs in a double-pulse trace is the following: By the induced charge in the detector by the first particle, the capacitor in the preamplifier circuit is charged up. The capacitor is then discharged due to the drain resistance circuit and the discharge follows an exponential decay. As the induced charge, due to the second particle, reaches the capacitor, it is charged again and the same exponential decay of the charge starts again. In the estimate of τ the single pulse occurs around channel 500. Consider the trace in Figure 5.1a. Here the second pulse starts to decay at around channel 3200 and therefore, in the deconvolution, it is necessary to employ the τ presented in Figure 5.15 shifted $3200 - 500 = 2700$ channels to the right.

Saturated traces as the one in Figure 5.2 need to be treated by the routine as well. These are a result of very energetic particles depositing their energy in the detectors. The

voltage capacity of the capacitors employed in the preamplifiers is very large. Thus, even if it is not evident from the recorded traces, the saturated pulses should experience the same exponential decay as unsaturated traces. However, the saturated traces cannot be treated similarly with the MWD method. The deconvolution of a saturated trace is illustrated in Figure 5.17.

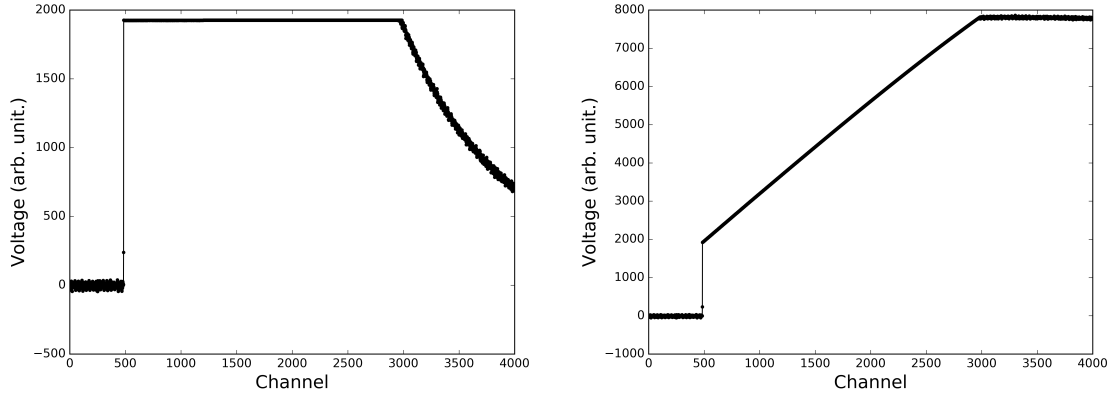

(a) **(b)**

Figure 5.17: (a) Baseline restored saturated trace **(b)** Deconvolution of (a). There are two features to highlight from the deconvolved trace, there is a linear growth as the trace is saturated and one can perhaps see that the plateau value seem to vary a little.

There is mainly one aspect that can be distinguished from Figure 5.17b. There is a linear growth for the channels which correspond to the saturation region of the original trace. From Equation (4.2) in Chapter 4 it is clear that if the preamplifier signal is constant the deconvolved trace will assume a linear behaviour with the slope $\frac{\Delta t}{\tau}$. This does not reflect the exponential decay present in the preamplifier signal and the obtained plateau height will not represent the real amplitude of the saturated pulse.

The matter can be solved by an extrapolation. Recall that the preamplifier decay can be represented by an exponential decay as presented in Equation (4.1) in Chapter 4. If the saturated height after a baseline restoration is denoted as A_{sat} and the time for which the trace is saturated is denoted sat_{dur}, the original height A can then be computed for a constant τ:

$$A = \frac{A_{sat}}{e^{-\frac{sat_{dur}}{\tau}}} \tag{5.3}$$

Pile-up traces in which one of the pulses was saturated for a fairly long time brought about a problem concerning the deconvolution. Such an example is illustrated in Figure 5.18. For this type of traces the deconvolution did not seem to work very well. Similar effects could also be noticed in other traces with pulses resulting in high preamplifier outputs, however not as distinct as with saturated traces. Since these traces did not occur very frequently and the effect on the obtained amplitudes were small, this was neglected further in this work.

5.3.2 Differentiation

An m-step differentiation was the next step in the MWD method. Originally, the purpose of this step is to restore the height of subsequent pulses in a pile-up trace (cf. Figure 4.1c)

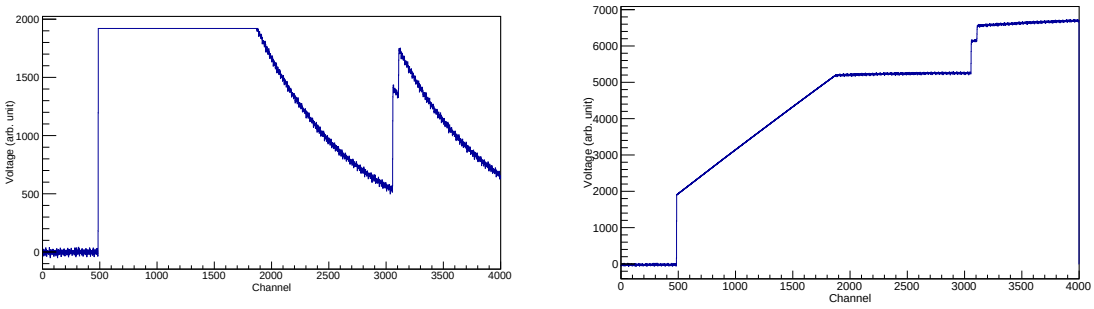

(a) **(b)**

Figure 5.18: (a) A saturated trace which contain three pulses. **(b)** Deconvolution of (a). From (b) it is clear that the last plateau is tilted.

and possibly also improve the amplitude with respect to the baseline. One could think it should not be necessary to include this step. Instead one could extract the amplitude of the first pulse and then the amplitude of the second pulse as its height in the deconvolved trace subtracted with the amplitude of the subsequent pulse. However, some testing showed this method was deemed too numerically unreliable. An implementation for a method, in which a differentiation with respect to the baseline was performed, was included to the routine.

A noise periodicity of 32-samples were discovered in the traces by U. Forsberg [3]. To further investigate this feature the variance was computed for the baseline (channels 64 to 450) with and without a 32-step differentiation. The variance of a 21-step differentiation and a 64-step differentiation was also computed in purpose of verification. The mean of the baseline variance for about 30000 traces are presented in Table 5.1.

Table 5.1: Mean baseline variance with and without differentiations. The baseline variance is computed as the variance of channels 64-450 and the mean of about 30000 computations is presented.

	Baseline variance
No differentiation	240
32-step differentiation	65
64-step differentiation	80
21-step differentiation	610

From Table 5.1 it is evident that the estimation in periodicity of 32 samples present in the noise is correct. Both the baseline variance of the 32- and 64-step are significantly smaller than the baseline variance without a differentiation.

By first performing an $n \cdot 32$-step differentiation on the deconvolved trace such that $n \cdot 32$ is larger than the width of the moving window w but smaller than t_{rise} the noise should be suppressed and a better average should be able to be computed. To test this hypothesis, one amplitude based on an $n \cdot 32$-step differentiation was implemented.

Further in this report the method in which the $n \cdot 32$-step differentiation with respect to the baseline is performed is referred to as *Method I*. The other method in which an n-step differentiation, where n depends on the width of the plateau is denoted *Method II*.

5.3.3 Averaging

To remove the noise a moving average is performed in the MWD method. It is unnecessary to compute a moving average over the complete trace as it is sufficient with only one value. This value should be computed as the average of as many samples (recall the length of the window w) on the plateau as is appropriate/possible. There are mainly three factors to take into account to determine w:

- An overshoot
- Number of samples to a subsequent pulse (if any)
- Where is the deconvolved trace most accurate

Based on these factors a routine was determined. For a pile-up trace each pulse was handled separately. For each pulse, the time difference (t_{diff}) between t_{fall} for the current pulse and t_{rise} for a subsequent pulse was computed. If a subsequent pulse was not present, the time difference towards the end of the trace was computed instead. Then, depending on the value of t_{diff} different averages were computed. However, if possible, the averaging was made a multiple of 32 values:

$$
\begin{array}{lll}
t_{diff} < 5 & \text{avg: } [t_{fall} : t_{fall} + t_{diff} - 1] & (1) \\
5 < t_{diff} < 20 & \text{avg: } [t_{fall} + 1 : t_{fall} + t_{diff} - 2] & (2) \\
20 < t_{diff} < 100 & \text{avg: } [t_{fall} + 2 : t_{fall} + t_{diff} - 4] & (3) \\
100 < t_{diff} < 400 & \text{avg: } [t_{fall} + 2 : t_{fall} + t_{diff} - 4] & (4) \\
t_{diff} > 400 & \text{avg: } [t_{fall} + 5 : t_{fall} + 389] & (5)
\end{array}
$$

A further motivation of the conditions might be suitable. If possible, the average should be computed over as many samples as possible. Thus, when there are very few samples available (point 1), it is appropriate to use all. If the time difference is sufficiently large (points 2, 3 and 4), the first channel which is included in the averaging is shifted to avoid including a very long overshoot. Finally, if there are a lot of samples available (point 4), the averaging is only computed over a maximum of 400 samples since the deconvolved trace is the most accurate here (cf. Figure 5.13). The implemented routine for a pile-up trace with two pulses with a small time difference is illustrated in Figure 5.19.

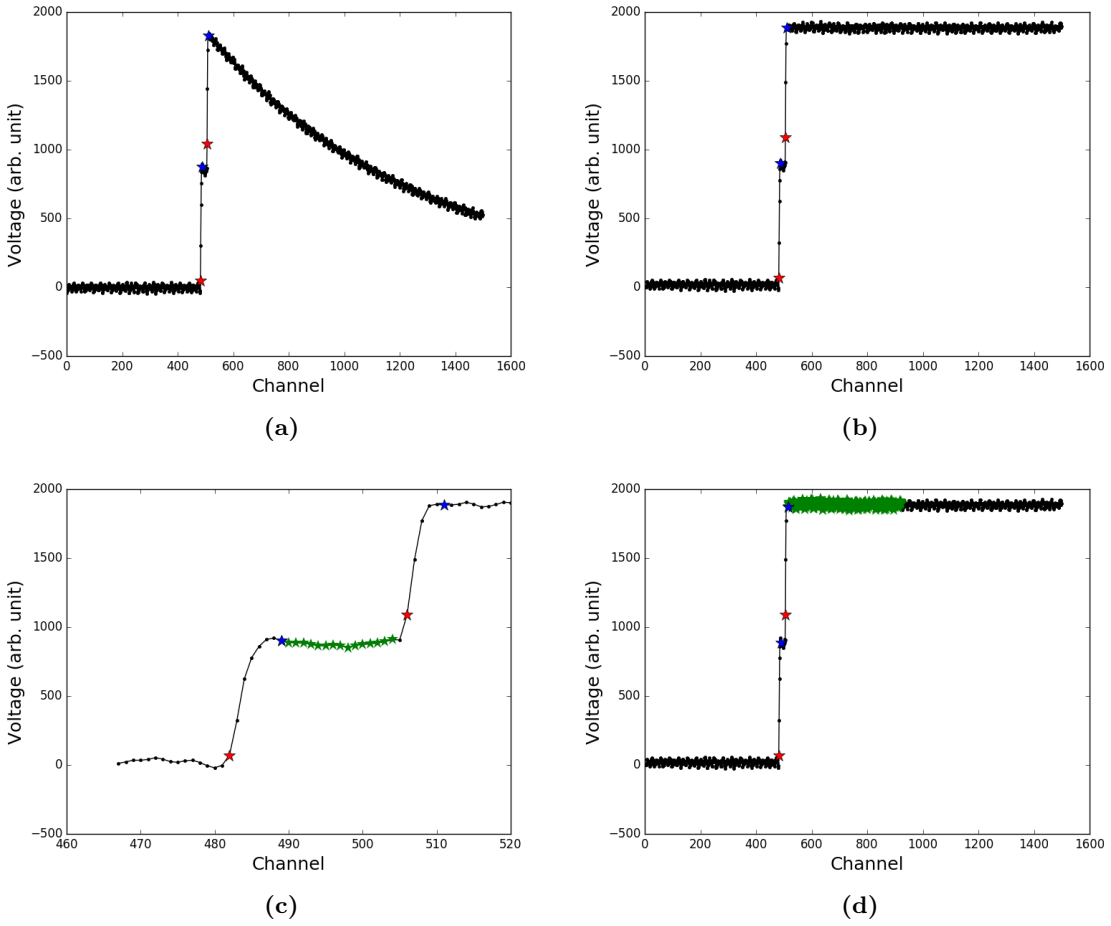

Figure 5.19: Illustration of the implemented routine which extracts amplitudes of pulses in pile-up traces. The red and the blue stars indicate t_{rise} and t_{fall} for the pulses, respectively. **(a)** double-pulse trace, to be handled by the routine. Firstly, t_{rise} and t_{fall} are evaluated as described in Section 5.1. **(b)** Deconvolution of the double-pulse trace. **(c)** deconvolved trace zoomed in to the region between the two pulses. The blue star followed by an array of green stars indicate the samples on which the average is computed for the first pulse. This average is then extracted as the amplitude of the first pulse. **(d)** The complete deconvolved trace. The blue star followed by an array of green stars indicate the samples on which the average is computed for the second pulse. The obtained average from this calculation is the total height of both pulses. The height of the second pulse is extracted as the value obtained from this average subtracted by the obtained height for the first pulse.

5.4 Implementation into the existing routine

The developed pile-up routine was included in the existing raw data handling routine, cf. Section 3.4.4, the following way. Traces from the p-strip were first processed with the filter described in Section 5.2. If the trace had more than 1 pulse it was treated with the developed pile-up routine, otherwise it was handled with the existing routine. To avoid unwanted oddly shaped pulses, an upper limit was set on the number of p-strips that had a signal. If four or more p-strips had signals the pulse was neglected for further analysis.

Chapter 6

Results

The developed pile-up analysis routine was employed for the entire E115-experiment dataset. The run took approximately three days to complete. All traces were filtered and the pulse amplitudes were calculated. Those amplitudes were translated into energies as described in Section 3.4.2. The results presented, concern those traces relevant to the newly developed routine, i.e. pile-ups. To begin with, some statistics and description of the employed search criteria from the experiment are presented. The obtained energy resolution with the developed routine is described. Next, the α-energies in the pile-up traces followed by α-decay lifetimes are calculated. In the second half of the chapter the focus lies on the connection of the obtained data to tabulated α-decay paths as a verification of the proper working of the entire method.

6.1 Search criteria and statistics

In order to find pile-up traces, specific search criteria (recall Section 3.4.4) were set to obtain pile-up traces containing i) one implant and one or two α-decays ii), just two α-decays iii) or three α-decays. The first α-decay in the pile-up traces will be referred to as α_1 and the second α_2 and so on, correspondingly. The criteria set for the decay correlations, for the result below in Table 6.1, were:

i) $11 \text{ MeV} < E_{\text{imp}} < 100 \text{ MeV}$

ii) $6 \text{ MeV} < E_{\alpha_{1\&,2\&,3}} < 11 \text{ MeV}$

iii) $\Delta t_{\text{imp-}\alpha_1},\ \Delta t_{\text{imp-}\alpha_2},\ \Delta t_{\alpha_1\text{-}\alpha_2},\ \Delta t_{\alpha_1\text{-}\alpha_3} < 66\ \mu\text{s}$

Unless otherwise mentioned, these search criteria were used in the presented results. In Table 6.1, some statistics from the E115-experiment data is presented.

Considering Table 6.1, the number of pile-up traces in comparison to the number of single-pulse traces obtained is rather large. Moreover, a big majority of them were α_1-α_2-pile-ups and these are the ones further analysed in this work.

Table 6.1: Statistics from the E115-experiment as obtained with the described search criteria.

Total number of traces	2.08×10^8
single-pulse	2.02×10^8
α_1-α_2	14 000
Implant-α_1	570
α_1-α_2-α_3	180

6.2 α_1-α_2-correlation spectra

As mentioned in Chapter 5, two methods were implemented as a part of the pile-up amplitude extraction routine. *Method I* is referred to the one with an $n \cdot 32$-sample differentiation whereas *Method II* is the one without it. In the α_1-α_2-correlation spectra in Figures 6.1 and 6.2, *Method I* has been used. In Figure 6.1 several blobs can be observed. This means that the implemented routine manages to reconstruct patterns in the data.

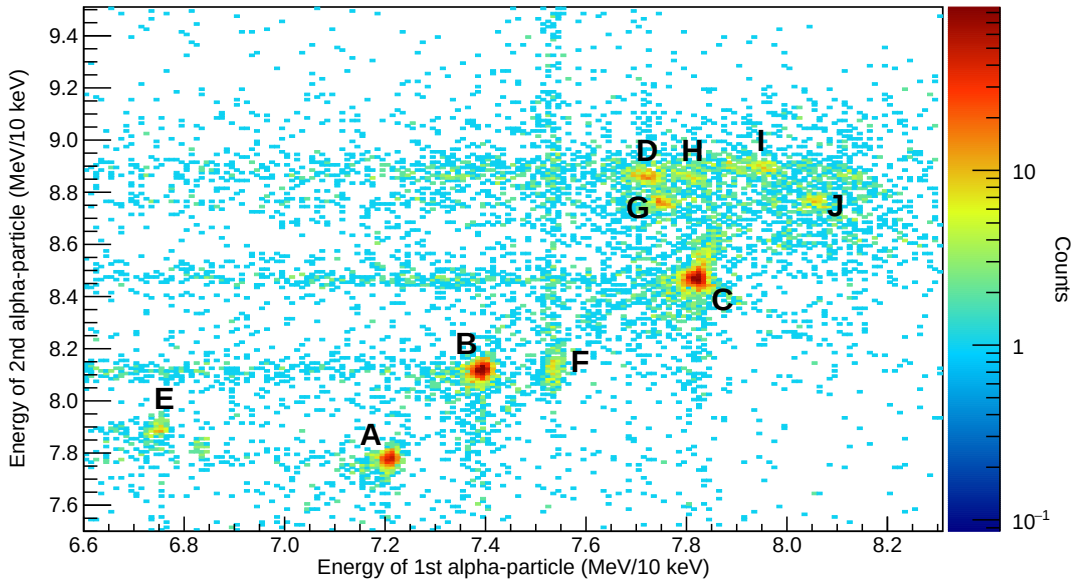

Figure 6.1: Energy of first α-particle, E_{α_1}, vs. energy of second α-particle, E_{α_2}. The different colors indicate the number of counts per pixel. Observed blobs are labelled with letters A-J.

In Figures 6.1 and 6.2, horizontal and vertical lines which proceed from the different peaks can be distinguished. In all cases except for one, the lines starts from the peak and moves to lower energies for either α_1- or α_2. From Figure 6.2 it seems like they origin from the peaks, as they assume similar mean lifetimes. What seems to be the case is: The full energy of one of the α-particles are measured whilst some of the energy of the other is lost or in one case energy is added.

If one considers E_{α_2} and the lifetimes of the decaying daughter, i.e. $\Delta t_{\alpha_1\text{-}\alpha_2}$, in Figure 6.2 one can see that as the energy increases, the lifetime decreases. This behaviour well reflects the principle of the Geiger-Nuttall law. The Geiger-Nuttall law roughly states that

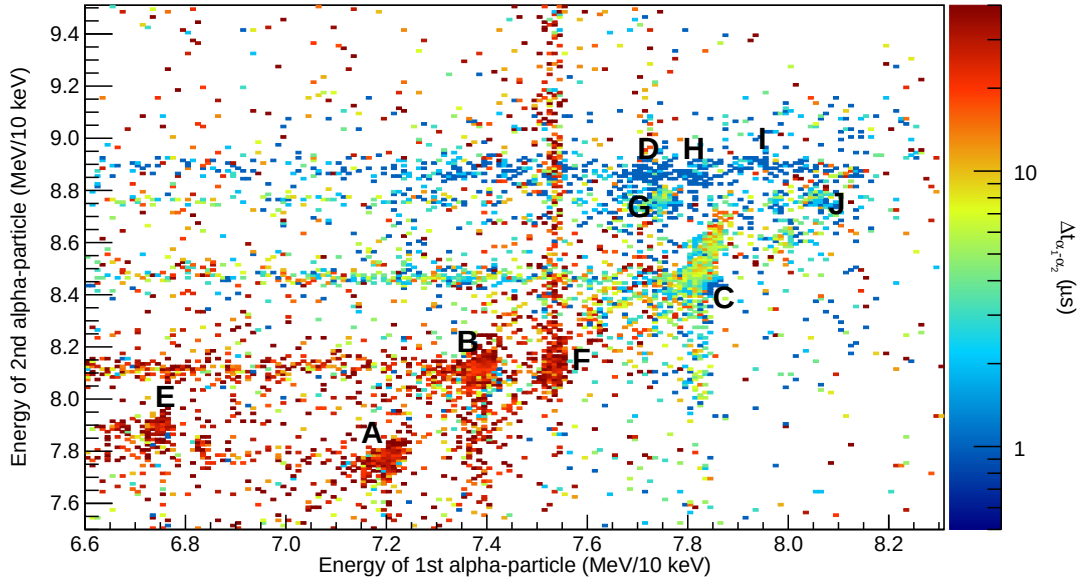

Figure 6.2: Energy of first α-particle, E_{α_1}, vs. energy of second α-particle, E_{α_2}. The different colors indicate the mean lifetime of the daughter nucleus of the first α-decay per pixel. Blobs identified in Figure 6.1 are indicated with letters A-J.

short-lived nuclei decays with the emission of more energetic α-particles, than those nuclei longer-lived [23].

6.3 Energy resolution

The determination of the α-particle energies in a pile-up trace was derived from the projections of a 2D-gate to the blobs in the α_1-α_2-energy spectrum presented in Figure 6.1. An example of a Gaussian fit to a projected energy peak is presented in Figure 6.3. In the fit process, different binnings were examined to optimise the fit. The width of the peak, i.e. the statistical uncertainty of the fit (1σ), is used in this report as the measurement uncertainty and it is also referred to as a measure of the experimental energy resolution.

In this work, this tail in Figure 6.3 and a seemingly small 2D-peak have been neglected and the analysis has only been focused on the largest peak.

The resolution, σ, of peaks A-D obtained with the two methods is presented as a function of energy in Figure 6.4. For *Method I* the resolution is also presented as a function of the mean lifetime of the complete 2D-peak in Figure 6.5. It is important to mention that *Method I* and *Method II* generated very close α-energy values. The maximum energy difference between the two methods for blobs A-D was about 6 keV, for an $E_\alpha = 8.87$ MeV.

From Figure 6.4 there is no clear preference for the energy resolutions between *Method I* and *Method II*. By comparing E_{α_1} and E_{α_2} the resolution is better for E_{α_1} in all cases except for region D. Furthermore, if one only considers regions A-C it is possible to distinguish a linear behaviour of the energy resolution as a function of energy.

Figure 6.5 illustrates the overall decrease in energy resolution as the mean lifetime of the

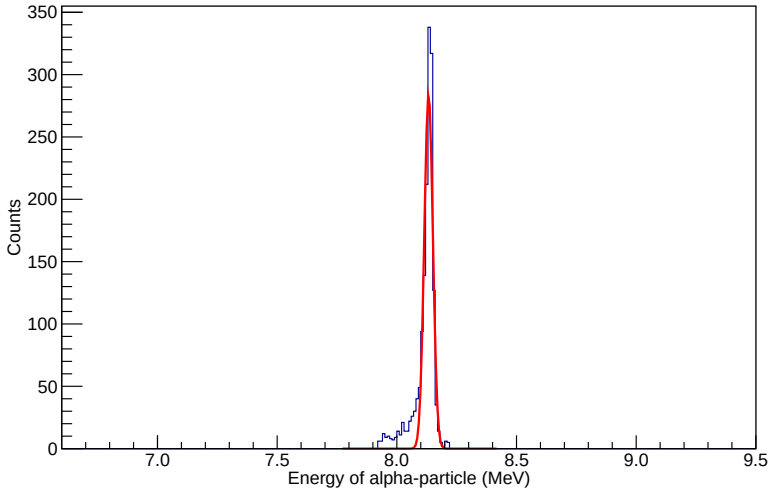

Figure 6.3: Example of the projection after the 2D-gate. A Gaussian fit is shown for demonstration purposes.

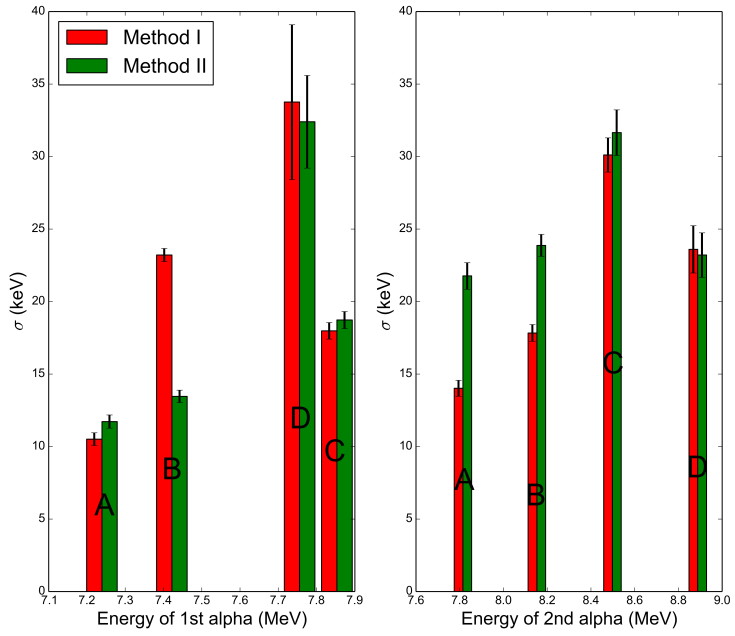

Figure 6.4: Energy resolution comparison between the two methods developed as depicted in the legend for regions A-D for α_1 (left) and α_2 (right).

peak decreases. However, fluctuations can be observed and the pattern is not very clear.

The best energy resolution with *Method I* was found for region A, with a mean lifetime of 18 μs, where the average with respect to E_{α_1} and E_{α_2} was at about 12 keV. The worst energy resolution was that of region D, where the mean lifetime was just short of 1 μs, with

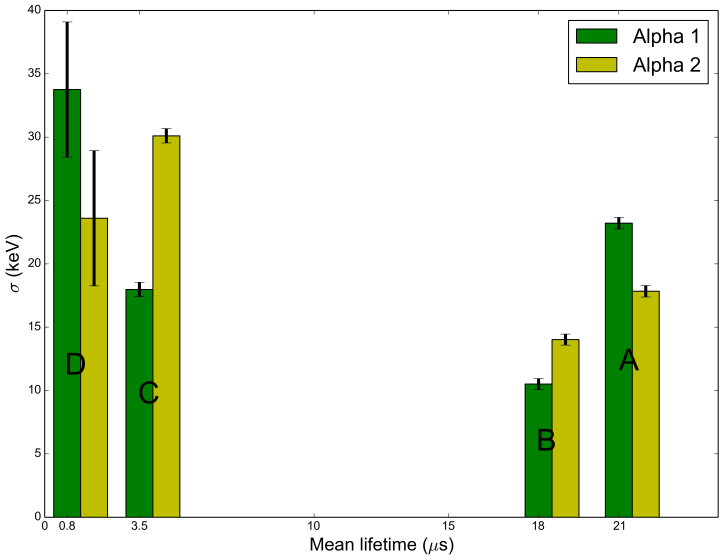

Figure 6.5: Energy resolution in regions A-D as a function of the mean lifetime for *Method I*.

an average for *Method I* at around 27 keV.

6.4 Half-life determination

For each singled out region, the time difference between the two α-particles was fitted to an exponential function $Ae^{-\lambda t}$ and the half-life was computed as $T_{1/2} = \frac{\ln 2}{\lambda}$. In the process the fitting, different binnings were examined to optimise the uncertainty. This turned out more challenging than anticipated as small changes could imply relatively large differences in the obtained half-life.

The uncertainty of the computed half-lives was obtained from the statistical uncertainty in the estimate of λ and Gauss' approximation:

$$V(g(\lambda)) \approx [g'(E(\lambda))]^2 V(\lambda), \tag{6.1}$$

with V as the variance. Moreover, $T_{1/2} = g(\lambda) = \frac{\ln 2}{\lambda}$, E is the expected value and g' is the first derivative of function g with respect to λ. The exponential fits for region B and G are presented in Figure 6.6.

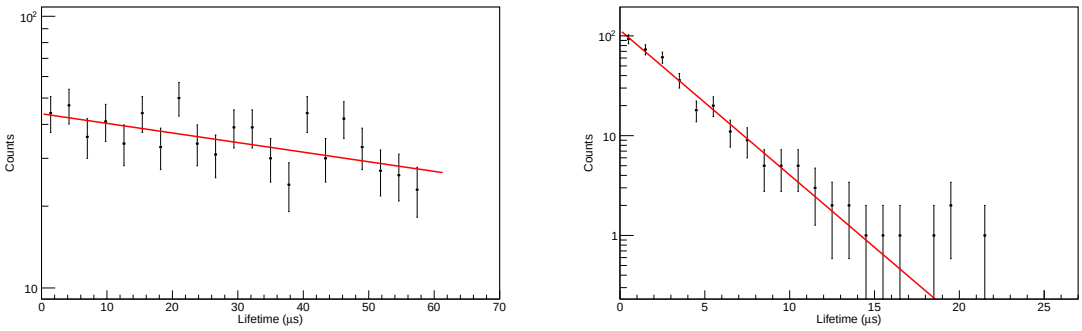

(a) Peak B. **(b)** Peak G.

Figure 6.6: Exponential fit (red) to the time difference data between α_1 and α_2, $\Delta t_{\alpha_1\text{-}\alpha_2}$, in the pile-up traces in regions B and G (black dots). The uncertainty in every point is presented with black capped bars. Note the log-scale on the y-axis. The resulting half-life estimates is 32(2) μs in **(a)** and 2.1(1) μs in **(b)**.

The selected $\Delta t_{\alpha_1\text{-}\alpha_2}$-data, depending on the region, followed an exponential distribution, as can be seen from Figure 6.6. The shorter the half-life of the data set, the better was the resemblance. The presented uncertainties in the following section well strengthens this statement. The reason for this could be that the upper limit of the time-data is set by the length of the recorded traces ($\sim$ 70 μs) and hence longer lifetimes have been neglected in the present analysis. However, since the purpose of this work is to study short-lived nuclei, no further effort was put in addressing this.

6.5 Compiled results

The properties of the regions, E_{α_1}, E_{α_2} and half-lives of the observed decays, are presented in this section. The energy values presented have been corrected for phonon excitation of the silicon lattice (see Section 3.4.2). It has been assumed that the average mass number of the decaying nuclei is 220. This corresponds to a correction of $\sim$ 70 keV.

For further analysis, to connect the fast α-decaying nuclei to a certain decay path, it is advantageous to know the energy of a subsequent α-decay, if there is one. To obtain this

energy, denoted E_{α_3}, 2D energy gates for E_{α_1} and E_{α_2} for different regions A-J were set. Furthermore, the time gate between α_2 and α_3 was adjusted to $\Delta t_{\alpha_2\text{-}\alpha_3} < 200$ s to search for longer correlation times.

In Table 6.2 the total number of counts for each peak is presented. This value represents the number of counts obtained when the 2D energy gate has been applied. As can be noted from Figure 6.3, the gating-procedure comes so clean that the background contribution is negligible.

Table 6.2: Compiled results for regions A-J as labelled in Figure 6.1. $E_{\alpha_{1,2,3}}$ indicate the energy of the first, second and third α-particle. $T_{1/2}$ represents the half-life of the second α-decay. The dashes indicate that no peak was found.

Region	E_{α_1} (MeV)	E_{α_2} (MeV)	$T_{1/2}$ (μs)	Total counts in region	E_{α_3} (MeV)
A	7.15(1)	7.72(1)	85(22)	758	-
B	7.33(2)	8.06(2)	32(2)	1602	6.62(1)
C	7.76(2)	8.41(3)	3.6(1)	2050	-
D	7.67(3)	8.80(2)	0.90(5)	432	-
E	6.69(2)	7.84(1)	44(12)	170	-
F	7.48(1)	8.07(3)	62(26)	249	-
G	7.68(5)	8.70(3)	2.1(1)	433	7.45(2)
H	7.75(3)	8.80(3)	0.7(1)	230	-
I	7.88(4)	8.83(3)	0.72(7)	323	-
J	8.00(3)	8.69(3)	1.9(2)	206	7.45(1)

From the plain Table 6.2 itself one cannot say much. The experimentally obtained data needs to be compared to already established data. Perhaps the most interesting feature of this table, is the absence of α_3 in the majority of cases. This is unexpected, but it can have many explanations. The resulting nuclei after the two α-decays might be stable one, it might decay with emission of a β-particle or electron capture or have a longer lifetime than the upper limit set in the search criterion.

6.6 Connection to decay paths

Once determined the properties of all the peaks, as presented in Table 6.2, it is possible to associate these to tabulated decay paths. In this work, one firmly established decay path is presented, see Figure 6.7. This connection works as a proof-of-concept for the developed method and sets the path for the feasibility of further analysis of the entire set of regions found.

The values from Table 6.2 were the basis for the connection, through regions G and J, to the decay of Ra-219. The accessibility of a subsequent third α-decay facilitated the connection.

For further confirmation of this decay path, γ-ray coincidences to the fast α-decays were studied. No coincidences to region J, neither with α_1 nor α_2 were found. For region G no coincidences were noticed for α_2, but a clear γ-coincidence peak could be seen at 316 keV for α_1. Evidence of this peak is illustrated in Figure 6.8. A comparison of the results from this work compared to previously measured data is presented in Table 6.3.

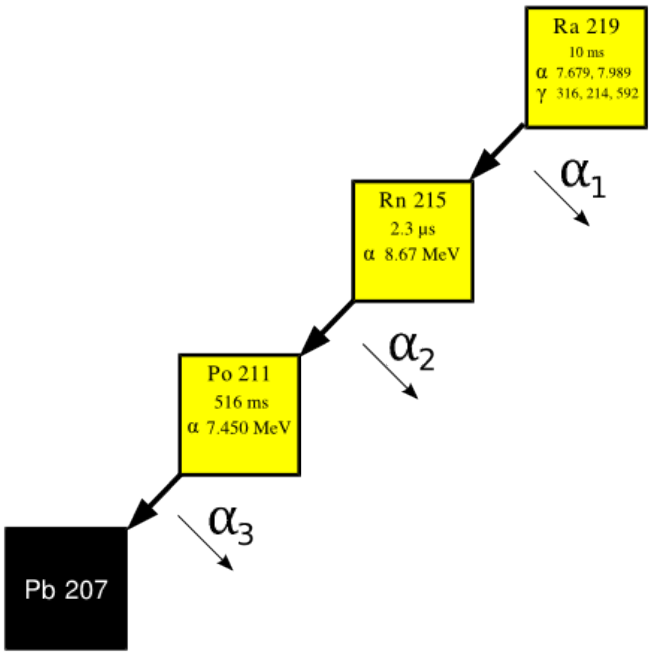

Figure 6.7: Tabulated α-decay path of Ra-219. The yellow filled squares indicate the α-decaying mode. The black filled square indicates that the nucleus is stable towards any decay. Previously measured data of α-decays, half-lives and γ-rays, relevant to this work, is presented within the respective boxes. If not explicitly indicated, E_α is presented in MeV and E_γ in keV. Image based on Ref. [33].

Incorporating the γ-decay, a decay level-scheme can be constructed based on the measurements from this work and is presented in Figure 6.9. The suggested scheme can be explained as follows: the ^{219}Ra nucleus is in its ground state and decays either to an excited state in the daughter ^{215}Rn or its ground state. The excited ^{215}Rn nucleus decays by emitting a γ ray. Lastly, ^{215}Rn in its ground state α-decays with a half-life of 2.0(1) μs to the ground state of ^{211}Po.

The congruence between the tabulated data and that from this work is quite good. All the α-decay energies and the γ-ray energy coincide with the tabulated data within experimental uncertainties. The half-life values do not match as good. However, the congruence to the tabulated half-life is within 3σ.

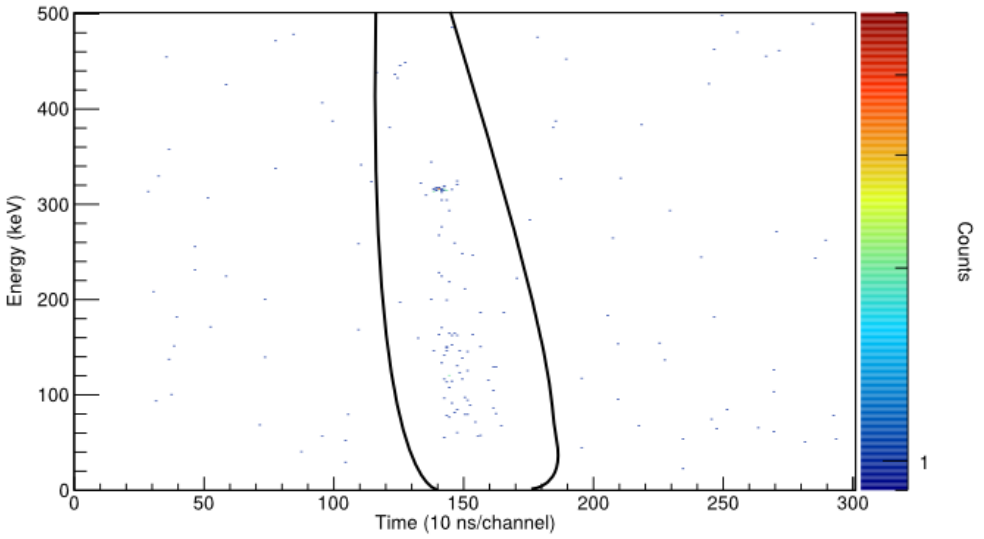

Figure 6.8: Prompt-coincidence window of the detected γ-rays gated on region G. Channel 100 corresponds to the event trigger time. The marked region indicates the prompt-coincidence window. A γ-peak at 316 keV can be observed within the coincidence window.

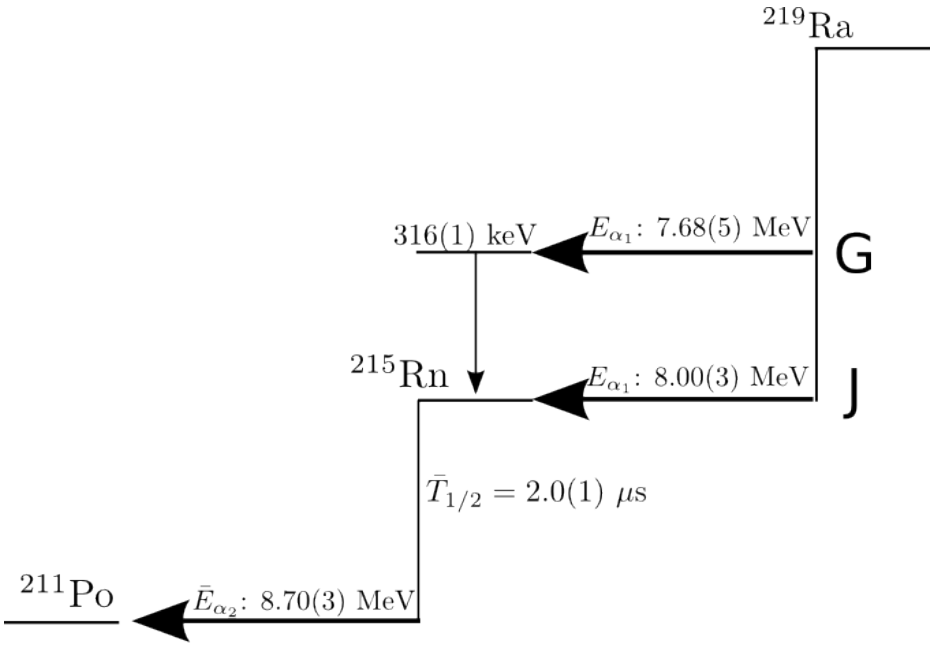

Figure 6.9: A decay level scheme of the ^{219}Ra decay constructed on the basis of the data obtained in this work. $\bar{E}_\alpha$ and $\bar{T}_{1/2}$ indicates that the combined data from both region G and J have been used.

Table 6.3: Compiled results for the identified decay path ^{219}Ra-^{215}Rn(-^{211}Po). Empty spots indicates potentially irrelevant tabulated data, as it was not measured in this work. A dash indicates that no data exists. The combined data for regions G and J is here presented for $T_{1/2}$ and E_α in the third column for ^{215}Rn.

Nuclide	Tabulated data [6]			This work		
	E_α (MeV)	$T_{1/2}$	γ (keV)	E_α (MeV)	$T_{1/2}$	γ (keV)
^{219}Ra						
	7.678(3)	10(3) ms	315.82(4)	7.68(5)		316(1)
	7.988(3)	10(3) ms	-	8.00(3)		-
^{215}Rn						
	8.674(8)	2.30(10) μs	-	8.70(3)	2.1(1) μs	-
			-	8.69(3)	1.9(2) μs	-
Combination			-	8.70(3)	2.0(1) μs	-
^{211}Po						
	7.4503(5)	516(3) ms		7.45(2)		
				7.45(1)		

Chapter 7

Discussion

The energy and time extraction of digitised preamplifier traces was performed with the pile-up analysis routine described in Chapter 5. In the development of the routine, different types of traces from the E115-experiment, were studied. During this process the characteristics of physically meaningful traces, single-pulse, pile-up and saturated traces were determined. This was important for a first stage filtering method which had the purpose to solely identify physically meaningful pile-up pulses, and reject oddly shaped pulses.

An important objective of the filtering method was to determine the time at which a pulse occurred, t_{rise}, the time at which the exponential decay of the pulse started, t_{fall}, and the corresponding parameter for t_{fall} in a saturated trace, t_{sat}. After some fine tuning, the desired values were obtained.

The biggest limitation with the developed pile-up filter was that the amplitude of a pulse needed to be sufficiently large, limited by the set threshold at the digital number 60, in order to be detected as a pulse above the noise and pass the filter. This has the consequence that pile-up events in two neighbouring strips or escaping pile-ups (cf. Figure 5.9) can have been neglected. This means that pile-up traces might not have been treated the way they should have and/or they might not have passed the filter which in turn should imply that some potentially interesting data was neglected. Another consequence is that the routine is not sensitive to other interesting decay modes, such as internal conversion.

Deviations from the flat plateaus in the deconvolution could be observed in the deconvolution of saturated pulses with subsequent pulses. A reason for this might be that the preamplifier behaves slightly different for high voltages. From Equation (4.2) it is actually quite obvious that the larger the preamplifier signal is the larger the compensation factor for the exponential decay becomes. Hence, the more sensitive the deconvolution becomes to the estimate of τ. In the current estimate of τ none of the saturated traces are included. To incorporate for a different behaviour, saturated traces should be modeled in a similar way as it was done for single-pulse traces (see Section 5.3.1). For the purpose of this work, a potential improvement for saturated traces should not be prioritised since the vast majority of interesting traces were α_1-α_2 pile-ups.

The MWD method was applied to extract the amplitudes in pile-up traces. The deconvolution part of the method was deemed especially important and a lot of work was put into optimising this step. Through a statistical analysis, a mix of a first order polynomial and a fourth degree polynomial fit to the exponential decay of the preamplifier was found to result in the best fitting and further also the best deconvolution. With this approach the

exponential decay constant τ became a function of the channel in the trace. This had the consequence that a shift was needed to be introduced to τ in the deconvolution of pile-up traces. In the differentiation part of MWD it was concluded that a $32 \cdot n$-step differentiation should be preferred due to the periodicity present in the electronic noise. In the same process, two slightly different methods was developed and compared.

The range on which the average, w, of the deconvolved and differentiated pile-up trace, was calculated and determined with t_{rise} and t_{fall}. Depending on the time differences between t_{fall} of a first pulse and t_{rise} of a second pulse, w was chosen and whenever possible it was determined as a multiple of 32 samples.

A possible future improvement to the newly developed pile-up routine should be considered a decreased threshold (currently set at the value 60) in the filtering method. With a lower threshold noisy traces will be identified as pile-ups. To be able to reject these noisy traces an iterative MWD procedure is proposed. By iterative I mean, that a trace is processed by the filter and then by the MWD routine, at least twice. In this way, noisy pulses can be neglected through a small obtained value with the MWD method in a first iteration and in a second iteration t_{rise} and t_{fall} can be adjusted and the proper values can be obtained with the MWD routine in a second iteration.

From an experimental point of view, improvements to the set-up, such as an ADC with more digital bits and higher sampling frequency of the digitisers, a faster charge of the capacitor in the preamplifier circuit and an ADC-range optimised for the polarity of the pulses, are desired.

The number of pile-up traces, around 15000, found in the E115-experimental data in comparison to single-pulse traces, $2 \cdot 10^8$, is not big. However, as shown in this work, this number is enough to perform data analysis.

The performance of the developed routine is quite good (see e.g. Figures 6.4) and 6.5. In Ref. [7] the resolutions in σ were with time differences down to 1 μs and 0.17 μs, ≈ 45 keV and ≈ 75 keV. Consider *Method I*. The worst resolution (E_{α_1} vs. E_{α_2}) was ~ 15 keV for region B with a mean lifetime of about 18 μs, while for region D with a mean lifetime of about 1 μs it was less than 30 keV. Thus, the routine delivers peak resolutions comparable to those in Ref. [7]. It is very difficult to conclude if any of the two methods outperforms the other as presented in Section 6.3. However, *Method I* was selected.

The main result of this work is illustrated in the α-α-correlation spectrum in Figure 6.1. Here the energy of the first α-particle is presented vs. the energy of the second α-particle for all analysed pile-up traces. The evidence of at least ten blobs in this 2D spectrum is evidence of that the developed routine can reconstruct patterns in the data.

Another verification of the developed routine, as it concerns extracted times, is that the obtained lifetimes for a region follow an exponential curve. This is well achieved for the ten regions. The half-lives of the acknowledged peaks were obtained through exponential fits.

The ten regions, A-J from Figure 6.1, were chosen for further studies. Many of the measured properties of these regions were compiled and presented in Table 6.2.

The compiled results for all regions were compared to tabulated nuclear decay data for the anticipated region illustrated in the introduction in Figure 1.1. Regions G and J could together be connected to the decay path of Ra-219. The presence of E_{α_3} for the two regions simplified the connection. Furthermore, coincident γ rays were found to one of the decays and could function as a verification that in fact this decay path had been found.

Tabulated decay properties of the Ra-219 decay are compared to values obtained in

this work in Table 6.3. All α-decay- and the γ-ray energies are congruent. The half-life values deviate a little. The tabulated half-life is 2.30(10) μs compared to 2.0(1) μs in this work. The difference is not larger than the 3σ error width. However, the tabulated half-life value was obtained from measurements performed in 1970 with an analogue pulse processing system with a lower limit of 2 μs [9]. Thus the value obtained in this work, 2.0(1) μs, is confidently an improved half-life of ^{215}Rn.

The obvious extension of this work is a continued study of the remaining eight (possibly even more), blobs presented in Figure 6.1 and connect these to decay paths. To the extension can be added three loose ends that were briefly mentioned in this report. The lines extending from the peaks in the α_1-α_2-correlation spectrum is one loose end. Two others are the tails that were clear in the 1D-peak spectrum and the missing α_3. The loose ends could potentially contain information of the nuclear structure of decay paths or be explained by physical consequences due to the experimental set-up and data analysis.

What could be found with the newly developed routine applied to the E115-experimental data, in the near future, is probably not new isotopes but rather improved branching-ratio measurements such as new γ-ray detections and decay modes. The search for non-tabulated data requires a more detailed study and therefore a lot of time. In this way, the thesis could set the path for future interesting research.

Conclusion

This work sets the proof-of-concept of energy and time extractions with a digital pulse processing system with an algorithm routine to study the properties of short-lived α-decaying nuclei.

References

[1] S. G. Nilsson and I. Ragnarsson. *Shapes and Shells in Nuclear Structure*. Cambridge University Press, 1995.

[2] A. Sobiczewski. Closed Shells for Z>82 and N>126 in a Diffuse Potential Well. *Physical Letters*, 1966.

[3] Ulrika Forsberg. *Element 115*. PhD thesis, Faculty of Science, Lund University, 2016.

[4] D. Rudolph et al. Spectroscopy of Element 115 Decay Chains. *Physical Review Letters*, 2013.

[5] J.M. Gates et al. First Superheavy Element Experiments at the GSI Recoil Separator TASCA: The Production and Decay of Element 114 in the ^{244}Pu(^{48}Ca, 3-4n) Reaction. *Physical Review C*, 2011.

[6] National Nuclear Data Center. Chart of Nuclides. `http://www.nndc.bnl.gov/chart/`, 2016.

[7] J. Khuyagbaatar et al. The New Short-Lived Isotope ^{221}U and the Mass-Surface Near N= 126. *Physical Review Letters*, 2015.

[8] J. D. Bowman et al. Alpha Spectroscopy of Nuclides Produced in the Interaction of 5 GeV Protons with Heavy Element Targets. *Physical Review C*, 1982.

[9] K. Valli. Production and Decay Properties of Thorium Isotopes of Mass 221-224 Formed in Heavy-Ion Reactions. *Physical Review C*, 1970.

[10] W. R. Leo. *Techniques for Nuclear and Particle Physics Experiments*. Springer-Verlag, 1st edition, 1987.

[11] . `http://www.studypage.in/images/physics/ec/pn-junction.png`.

[12] . `http://hyperphysics.phy-astr.gsu.edu/hbase/solids/imgsol/bias10.gif`.

[13] U. Forsberg. Pulse Shape Analysis for Heavy Element Spectroscopy. Master's thesis, Division of Nuclear Physics, Lund University, 2010.

[14] S. Takeda et al. Double-Sided Silicon Strip Detector for X-ray Imaging. *SPIE Newsroom*, 2008.

[15] G. Duchene et al. The CLOVER: a New Generation of Gomposite Ge Detectors. *Nuclear Instruments and Methods in Physics Research A*, 1999.

[16] J. Eberth et al. Encapsulated Ge Detectors: Development and First Tests. *Nuclear Instruments and Methods in Physics Research A*, 1996.

[17] Ortec. Preamplifier Introduction. Technical report, `www.ortec-online.com/download/Preamplifier-Introduction.pdf`, 2008.

[18] Wikipedia. Flash ADC. `https://en.wikipedia.org/wiki/Flash_ADC`, 2016.

[19] D. Sjöberg & M. Gustafsson. *Kretsteori, ellära och elektronik*. Lunds Universitet, 5th edition, 2013.

[20] G. F. Knoll. *Radiation, Detection and Measurements*. John Wiley & Sons, Inc., 4th edition, 2010.

[21] C. Tintori. WP2081 Digital Pulse Processing in Nuclear Physics. Technical report, CAEN Nuclear Physics, `http://www.caen.it/documents/News/32/WP2081_digitalpulseprocessing_03.pdf`, 2011.

[22] J. Jeppsson. Techniques for Discovering and Identifying New Elements. Master's thesis, Division of Nuclear Physics, Lund Engineering Faculty, 2012.

[23] K. S. Krane. *Introductory Nuclear Physics*. John Wiley & Sons, 2nd edition, 1988.

[24] L. Corrade et al. Multinucleon Transfer Reactions in ^{40}Ca and ^{124}Sn. *Physical Review C*, 1996.

[25] L.-L. Andersson et al. TASISpec - A Highly Efficient Multi-Coincidence Spectrometer for Nuclear Structure Investigations of the Heaviest Nuclei. *Nuclear Instruments and Methods in Physics Research A*, 2010.

[26] J. Ziegler. The Stopping and Range of Ions in Matter (SRIM). `http://www.srim.org/`.

[27] GSI. The GO4 project page. `https://www.gsi.de/en/work/fairgsi/rare_isotope_beams/electronics/data_processing/data_analysis/the_go4_home_page.htm`, 2016.

[28] CERN. ROOT Data Analysis Framework. `https://root.cern.ch/`, 2016.

[29] A. Georgiev & W. Gast. Digital Pulse Processing in High Resolution, High Throughput Gamma-Ray Spectroscopy. *IEEE TRANSACTIONS ON NUCLEAR SCIENCE*, 1993.

[30] V. T. Jordanov & G. F. Knoll. Digital Synthesis of Pulse Shapes in Real Time for High Resolution Radiation Spectroscopy. *Nuclear Instruments and Methods in Physics Research A*, 1994.

[31] Martin Lauer. *Digital Signal Processing for segmented HPGe Detectors Preprocessing Algorithms and Pulse Shape Analysis*. PhD thesis, Combined Faculties for the Natural Sciences and for Mathematics of the Ruperto-Carola University of Heidelberg, Germany, `http://pubman.mpdl.mpg.de/pubman/item/escidoc:919015/component/escidoc:919014/Lauer-diss.pdf`, 2004.

[32] V. I. Stoica. *Digital Pulse-Shape Analysis and Controls for Advanced Detector Systems.* PhD thesis, Helmholtzzentrum für Schwerionrnforschung GmbH (GSI), Germany - KVI University of Groningen, Germany, `www.rug.nl/research/portal/files/14645846/proefschriftStoica.pdf`, 2012.

[33] Karlsruhe Nuclide Chart. `http://www.nucleonica.com/wiki/index.php?title=Category%3AKNC`.